Neuron
Article

An LRRTM4-HSPG Complex Mediates Excitatory Synapse Development on Dentate Gyrus Granule Cells

Tabrez J. Siddiqui,[1] Parisa Karimi Tari,[1] Steven A. Connor,[1,2] Peng Zhang,[1] Frederick A. Dobie,[1] Kevin She,[1] Hiroshi Kawabe,[3] Yu Tian Wang,[2] Nils Brose,[3,4,*] and Ann Marie Craig[1,*]
[1]Brain Research Centre and Department of Psychiatry
[2]Brain Research Centre and Department of Medicine
University of British Columbia, Vancouver, BC V6T 2B5, Canada
[3]Department of Molecular Neurobiology, Max Planck Institute of Experimental Medicine, 37075 Göttingen, Germany
[4]Center for Nanoscale Microscopy and Molecular Physiology of the Brain (CNMPB), 37073 Göttingen, Germany
*Correspondence: brose@em.mpg.de (N.B.), acraig@mail.ubc.ca (A.M.C.)
http://dx.doi.org/10.1016/j.neuron.2013.06.029

SUMMARY

Selective synapse development determines how complex neuronal networks in the brain are formed. Complexes of postsynaptic neuroligins and LRRTMs with presynaptic neurexins contribute widely to excitatory synapse development, and mutations in these gene families increase the risk of developing psychiatric disorders. We find that LRRTM4 has distinct presynaptic binding partners, heparan sulfate proteoglycans (HSPGs). HSPGs are required to mediate the synaptogenic activity of LRRTM4. LRRTM4 shows highly selective expression in the brain. Within the hippocampus, we detected LRRTM4 specifically at excitatory postsynaptic sites on dentate gyrus granule cells. *LRRTM4*$^{-/-}$ dentate gyrus granule cells, but not CA1 pyramidal cells, exhibit reductions in excitatory synapse density and function. Furthermore, *LRRTM4*$^{-/-}$ dentate gyrus granule cells show impaired activity-regulated AMPA receptor trafficking. These results identifying cell-type-specific functions and multiple presynaptic binding partners for different LRRTM family members reveal an unexpected complexity in the design and function of synapse-organizing proteins.

INTRODUCTION

Several *trans*-synaptic protein complexes that mediate axon-dendrite adhesion and local presynaptic and postsynaptic differentiation have been identified. The complement of synapse-organizing proteins at developing synapses—even in a cell-type-specific manner—may determine synaptogenesis by controlling initial axon-dendrite adhesion, morphological, molecular, and functional maturation of synapses, as well as synapse stability and plasticity. Many of these synapse-organizing complexes involve either presynaptic neurexins or type IIa protein tyrosine phosphatases (Krueger et al., 2012; Shen and Scheiffele, 2010; Siddiqui and Craig, 2011; Takahashi et al., 2011, 2012; Yoshida et al., 2011, 2012; Yuzaki, 2011), along with diverse postsynaptic binding partners.

LRRTM1 and LRRTM2, together with neuroligins and Cbln-GluRδ, are postsynaptic binding partners of presynaptic neurexins at glutamatergic synapses (Siddiqui and Craig, 2011). LRRTM1 was identified in an unbiased expression screen for synaptogenic proteins (Linhoff et al., 2009). When presented to axons on the surfaces of dendrites, nonneuronal cells, or beads, LRRTM1 and LRRTM2 potently induce glutamatergic presynapse differentiation at the axonal contact site, via neurexin binding (de Wit et al., 2009; Ko et al., 2009; Linhoff et al., 2009; Siddiqui et al., 2010).

Many of the excitatory synapse-organizing proteins are broadly expressed in overlapping brain regions, and evidence indicates that they may cooperate in synapse development. In hippocampus, for example, LRRTM1, LRRTM2, neuroligin-1, neuroligin-3, NGL-3, IL1RAPL1, TrkC, and their presynaptic binding partners are expressed by all excitatory neuron classes (Altar et al., 1994; Carrié et al., 1999; Kim et al., 2006; Laurén et al., 2003; Varoqueaux et al., 2006). Experiments involving simultaneous knockdown of LRRTM1, LRRTM2, and neuroligin-3 together with genetic deletion of neuroligin-1 revealed cooperative roles of these postsynaptic partners of neurexins in functional excitatory synapse development in hippocampal CA1 neurons (Soler-Llavina et al., 2011). In contrast, NGL-2 functions in a pathway-specific manner at subsets of hippocampal synapses (DeNardo et al., 2012). However, more generally, the molecular basis of pathway or cell-type-specific development of mammalian excitatory synapses is not well understood.

LRRTM4 was also found to induce excitatory presynapse differentiation with a similar potency as LRRTM2 (Linhoff et al., 2009), but its expression in brain is more restricted. LRRTM4 mRNA is expressed at very high levels in dentate gyrus granule cells and in the anterior olfactory nucleus and at low or moderate levels in other brain regions such as cortex and striatum (Laurén et al., 2003; Lein et al., 2007). Like genes encoding neurexins, neuroligins, and several other synapse-organizing proteins (Betancur et al., 2009; Südhof, 2008), *LRRTM4* is linked to autism spectrum disorders (Michaelson et al., 2012; Pinto et al., 2010), and in a recent genome-wide association study, *LRRTM4* was

linked to risk of attempted suicide in females (Willour et al., 2012). LRRTM4 was also recently isolated as a major component of native AMPA-type glutamate receptor complexes (Schwenk et al., 2012). However, in contrast to the rather extensive knowledge on LRRTM1 and LRRTM2, the molecular interactions and roles of LRRTM4 in synapse development have not been well studied.

We assessed the role of LRRTM4 in synapse development and show by targeted deletion in mice that LRRTM4 is essential for normal excitatory synapse development and function in dentate gyrus granule cells but not in CA1 hippocampal pyramidal neurons. Furthermore, we identify a family of new extracellular binding partners for LRRTM4, heparan sulfate proteoglycans (HSPGs), and show that HSPGs are essential to mediate the synaptogenic activity of LRRTM4. Thus, LRRTM family members function at different subsets of excitatory synapses and act through distinct molecular pathways.

RESULTS

LRRTM4 Localizes to Excitatory Postsynaptic Sites on Dentate Gyrus Granule Cells

In accordance with a possible role of LRRTM4 in synaptogenesis, western blot analyses of the developmental time course of LRRTM4 expression in whole-brain homogenates showed that LRRTM4 expression parallels the time course of synaptogenesis. LRRTM4 was readily detectable by postnatal day 6, and its levels increased until postnatal day 30 and then remained at a high level 1 month later (Figure 1A), indicating that LRRTM4 expression rises during the peak phase of synaptogenesis and then reaches a plateau.

Western blot analysis of biochemically isolated subcellular fractions from whole brain revealed an enrichment of LRRTM4 in the synaptic plasma membrane fraction and, along with the excitatory postsynaptic scaffold PSD-95 family, in the detergent-resistant postsynaptic density fraction (Figure 1B), indicating a synaptic localization of LRRTM4. To assess whether LRRTM4 may associate with excitatory postsynaptic components, mouse brain crude synaptosomal fractions were solubilized and immunoprecipitated with antibodies to PSD-95 family proteins and AMPA receptor subunit GluA1 antibodies. LRRTM4 coimmunoprecipated with both PSD-95 family proteins and GluA1 but not with control IgGs (Figure 1C). These results are consistent with a previous report showing that LRRTM4 is a component of native AMPA receptor complexes (Schwenk et al., 2012).

To further examine the subcellular localization of LRRTM4, we expressed LRRTM4 with an extracellular YFP tag in cultured hippocampal neurons (Figures 1D and 1E). YFP-LRRTM4 was trafficked to dendrites but not to axons. Within dendrites, YFP-LRRTM4 clustered at excitatory postsynaptic sites and colocalized with PSD-95 opposite to vesicular glutamate transporter VGlut1-positive terminals. YFP-LRRTM4 localization did not overlap with the localization of gephyrin or vesicular GABA transporter VGAT marking inhibitory synapses.

To assess the cellular and subcellular distribution of LRRTM4 in vivo, we generated an antibody against the intracellular domain of LRRTM4 suitable for immunofluorescence and validated it using mouse tissue lacking LRRTM4 (see Figures 6B). Consistent with the high level of LRRTM4 mRNA expression in dentate gyrus granule cells (Laurén et al., 2003; Lein et al., 2007) and sorting of YFP-LRRTM4 protein to excitatory postsynaptic sites, strong anti-LRRTM4 immunoreactivity was observed in hippocampal dentate gyrus molecular layers (Figures 1F and 1G). LRRTM4 was present throughout the molecular layer and slightly more concentrated in the inner molecular layer. Punctate LRRTM4 immunofluorescence overlapped with the localization of PSD-95 and the active zone molecule bassoon. Although LRRTM4 mRNA is expressed at lower levels in cortex, we did not detect clear immunoreactivity in cortex. Altogether, its subcellular localization and expression profile indicate that LRRTM4 operates at excitatory postsynaptic sites in dentate gyrus granule cells.

Overexpression of LRRTM4 Increases the Number of Excitatory Inputs

To study the role of LRRTM4 in synapse development, we first assessed effects of increasing the levels of LRRTM4 in cultured hippocampal neurons. Overexpression of YFP-LRRTM4 significantly enhanced clustering of presynaptic VGlut1 along transfected dendrites as compared with neighboring neurons or control neurons expressing CFP (Figures S1A–S1C available online). In contrast, VGAT clustering was not affected by YFP-LRRTM4 expression (Figures S1D and S1E). Thus, consistent with the ability of LRRTM4 to induce excitatory but not inhibitory presynapse differentiation in a fibroblast coculture assay (Linhoff et al., 2009), neuronal overexpression of LRRTM4 increases excitatory but not inhibitory presynaptic inputs.

The LRRTM4 Ectodomain Binds to HSPGs

To mediate its synaptogenic effect (Figure S1), LRRTM4 must directly or indirectly interact with presynaptic ligands. Given that LRRTM1 and LRRTM2 bind to and induce presynaptic differentiation through neurexins (de Wit et al., 2009; Ko et al., 2009; Siddiqui et al., 2010), we tested whether LRRTM4 also binds to neurexins. A soluble recombinant protein consisting of the laminin, neurexin, sex-hormone-binding globulin (LNS) domain of neurexin1β lacking the insert at splice site 4 fused to the human immunoglobulin constant region, neurexin1β(-S4)-Fc, bound to COS7 cells expressing Myc-LRRTM1 or Myc-LRRTM2 but, unexpectedly, not to cells expressing Myc-LRRTM4 (Figure S2). Binding of neurexin1β(-S4)-Fc to cells expressing Myc-LRRTM4 was not significantly different from binding to cells expressing the negative control Myc-SALM2 (Figure S2B).

We then performed an unbiased search for extracellular binding partners of LRRTM4. We generated a recombinant protein containing the ectodomain of LRRTM4, LRRTM4-Fc, and used this for affinity purification of ligands from a solubilized crude rat brain synaptosomal fraction (Figure 2A). Polyacrylamide gel analysis revealed specific proteins, particularly several with molecular weights around 52–72 kDa, that bound to and were eluted from a matrix bearing LRRTM4-Fc but not Fc control protein. Mass spectrometry analysis revealed glypican-1, glypican-3, glypican-4, and glypican-5 as components of the 52–72 kDa band (Table S1). Glypicans constitute a family of cell-surface

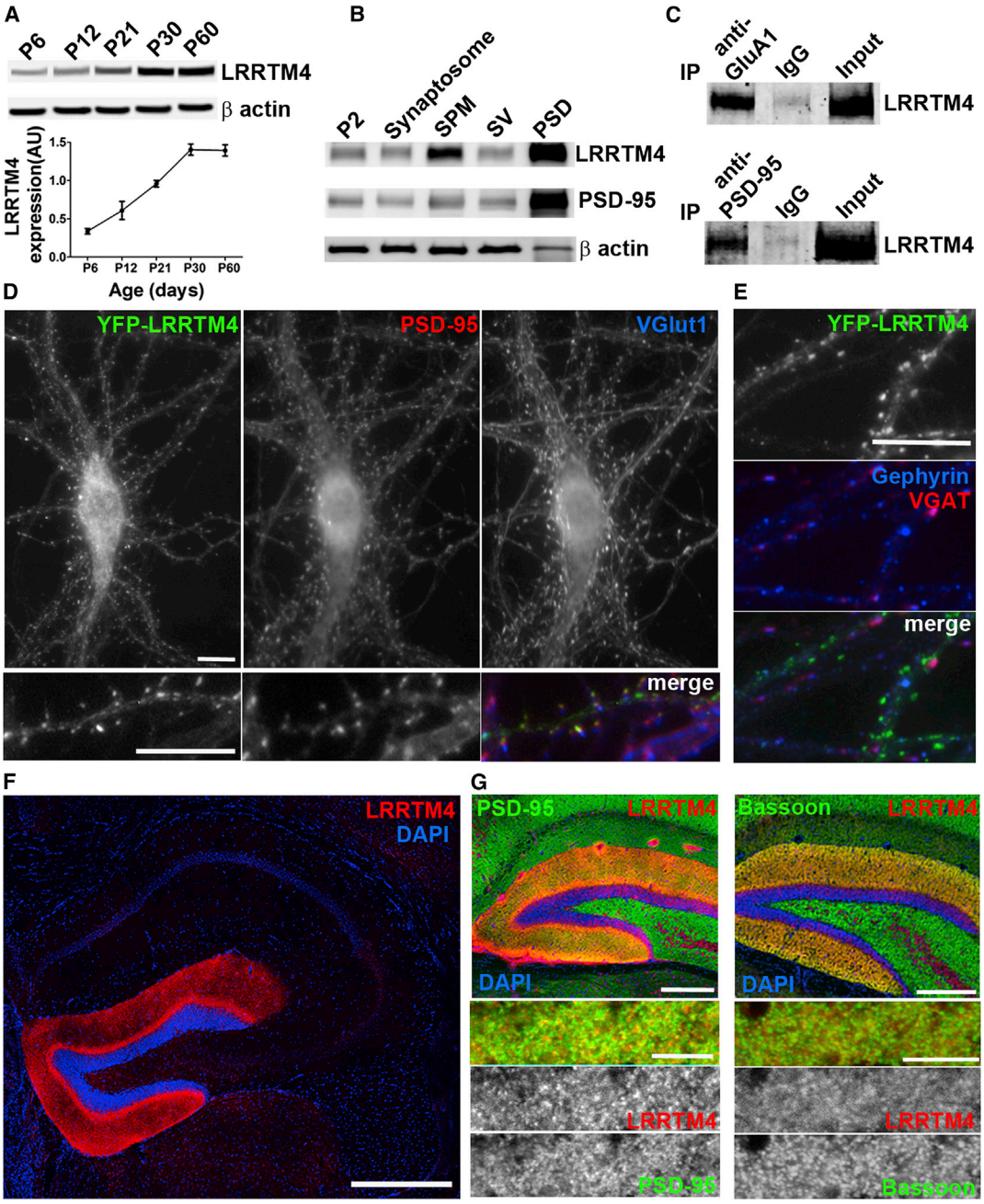

Figure 1. LRRTM4 Localizes to Excitatory Postsynaptic Sites on Dentate Gyrus Granule Cells

(A) Western blot analysis of LRRTM4 expression levels in mouse brain homogenates from postnatal day 6 (P6) to P60 and quantitation of the relative expression level of LRRTM4 in mouse brain homogenate during postnatal development. Data are presented as mean ± SEM of three to five experiments.

(B) Western blotting of synaptic fractions of adult rat brain homogenate shows that LRRTM4 is enriched in the synaptic plasma membrane (SPM) fraction and, along with PSD-95, in the postsynaptic density (PSD) fraction as compared with crude synaptosome (P2), synaptosome, and synaptic vesicle (SV) fractions.

(C) Immunoprecipitation from solubilized mouse brain crude synaptosomal fraction by anti-PSD-95 family and anti-GluA1 antibodies but not control IgG coimmunoprecipitated LRRTM4.

(D and E) YFP-LRRTM4 expressed at low level from 0–14 DIV in cultured hippocampal neurons concentrated at excitatory postsynaptic sites colocalized with PSD-95 and apposed to VGlut1 (D). YFP-LRRTM4 did not cluster at inhibitory synapses labeled with gephyrin and VGAT (E).

(F and G) LRRTM4 immunoreactivity in coronal sections of adult mouse brain was observed at highest levels in the dentate gyrus molecular layer and was not observed elsewhere within the hippocampus (F). Within the dentate gyrus, LRRTM4 was present in a punctate pattern showing overlap with PSD-95 and bassoon (G). This antibody was validated using tissue lacking LRRTM4 (Figure 6B).

Scale bars represent 10 μm in (D) and (E), 500 μm in (F), 250 μm in G (top), and 5 μm in (G) (bottom).

See also Figure S1.

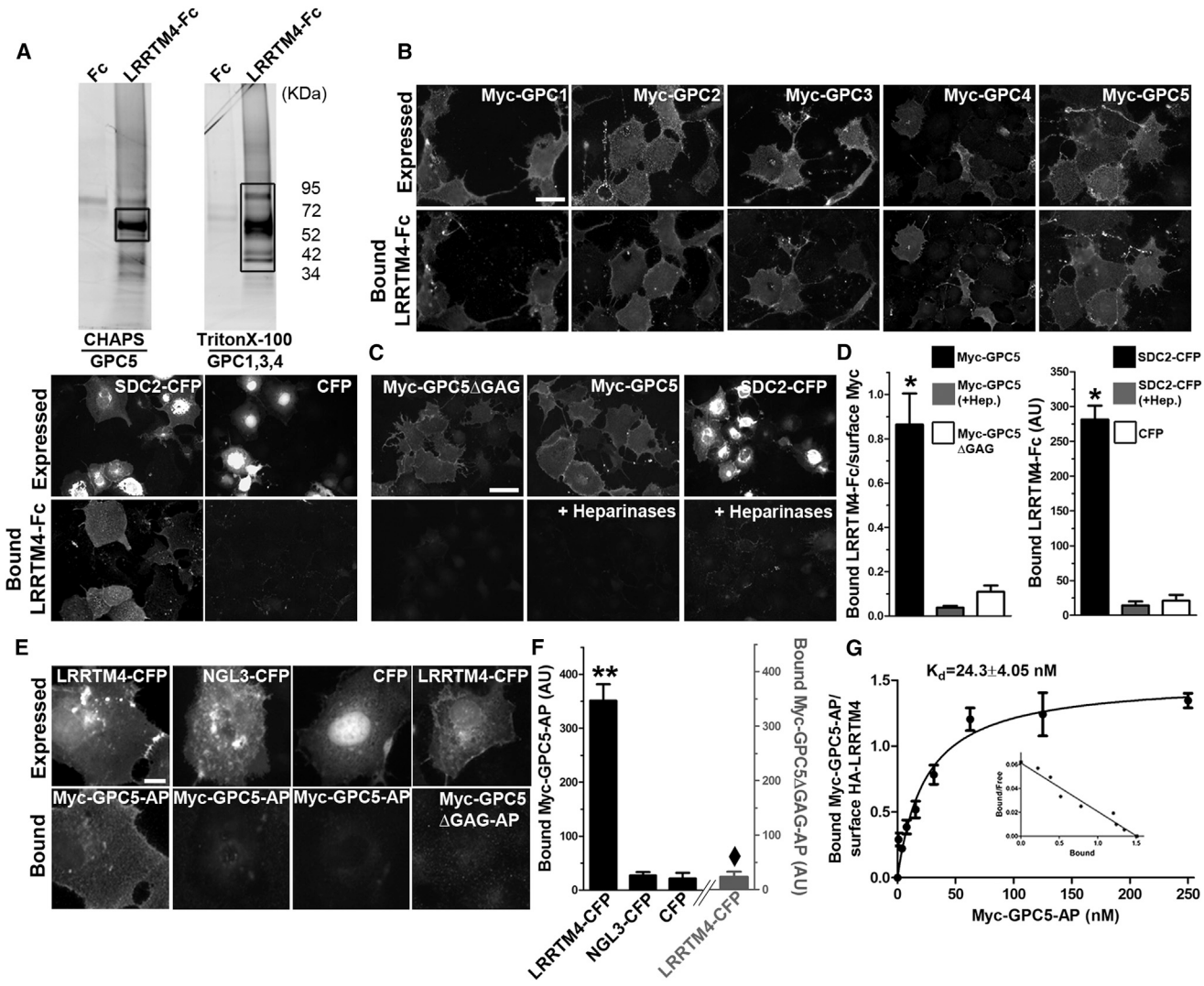

Figure 2. LRRTM4 Binds HSPGs

(A) SYPRO Ruby-stained gel shows proteins isolated by affinity chromatography with LRRTM4-Fc or control Fc from rat brain crude synaptosome fractions solubilized with the indicated detergents. Analysis of the boxed regions by liquid chromatography-mass spectrometry yielded the indicated glypicans as prominent components.

(B–G) Candidate proteins were expressed in COS7 cells and tested for binding of the indicated Fc or AP fusion protein. Expressed myc-tagged proteins were visualized by surface labeling.

(B) Upon expression in COS7 cells, all glypicans (GPCs) and syndecans (SDCs) tested mediated strong binding of LRRTM4-Fc. A much lower level of LRRTM4-Fc binding to neighbor-untransfected or CFP-transfected COS7 cells was also frequently observed.

(C) The HS-deficient mutant GPC5ΔGAG did not mediate binding of LRRTM4-Fc. Treatment of the cultures with heparinases to cleave the HS chains eliminated the binding of LRRTM4-Fc to COS7 cells expressing GPC5 or SDC2 and eliminated the low-level binding to neighbor-untransfected cells.

(D) Quantitation of LRRTM4-Fc binding to COS7 cells expressing the indicated constructs. ANOVA $p < 0.0001$, $^{*}p < 0.05$ compared with Myc-GPC5ΔGAG or with CFP by Tukey's multiple comparison test, n = 15 cells each.

(E) Upon expression in COS7 cells, LRRTM4-CFP, but not NGL-3-CFP or CFP controls, mediated binding of Myc-GPC5-AP but not the HS-deficient mutant Myc-GPC5ΔGAG-AP.

(F) Quantitation of bound glypican-5 fusion protein (left y axis, black) or HS-deficient mutant (right y axis, gray) to COS7 cells expressing the indicated constructs. ANOVA $p < 0.0001$, $^{**}p < 0.001$ for binding of Myc-GPC5-AP compared with CFP control by Tukey's multiple comparison test, ◆ $p < 0.001$ comparing binding of Myc-GPC5-AP and Myc-GPC5ΔGAG-AP to LRRTM4, n = 10 cells each.

(G) By Scatchard analysis, the K_d of binding of Myc-GPC5-AP to cell-expressed HA-LRRTM4 was estimated at 23.4 nM (n = 9 cells each).

Data are presented as mean ± SEM. Scale bars represent 50 μm in (B) and (C) and 10 μm in (E).

See also Figure S2.

glycophosphatidylinositol (GPI)-anchored HSPGs with six family members, all of which are expressed in the CNS (Fransson et al., 2004). Like other HSPGs, glypicans contain protein backbones that are covalently conjugated to heparan sulfate (HS) glycosaminoglycan chains.

To test whether LRRTM4 and glypicans interact directly, we expressed Myc-tagged glypican-1–glypican-5 individually in COS7 cells and incubated these with LRRTM4-Fc. COS7 cells expressing any of the glypicans tested showed strong binding of LRRTM4-Fc, while control cells did not (Figure 2B). To determine whether binding was specific for glypicans, we tested syndecan-2 (SDC2) as a representative syndecan and also observed strong binding of LRRTM4-Fc to cells expressing SDC2-CFP. We next tested whether the HS chains on glypicans or SDC2 are essential for LRRTM4 binding. Binding to COS7 cells expressing glypican-5 (GPC5) or SDC2 was abolished by treatment of the expressing cells with heparinases that cleave the HS chains (Figures 2B–2D). Consistent with this result, LRRTM4-Fc did not bind to the surface of COS7 cells expressing a mutant of GPC5 that lacks the five serine residues involved in glycosaminoglycan linkage and cannot be glycanated (GPC5ΔGAG) (Figures 2C and 2D). We then performed a reciprocal assay to confirm the interaction between LRRTM4 and HSPGs (Figures 2E–2G). A recombinant protein consisting of a Myc-tagged ectodomain of GPC5 fused to alkaline phosphatase, Myc-GPC5-AP, but not the Myc-tagged nonglycanated GPC5 (Myc-GPC5ΔGAG-AP), bound specifically to COS7 cells expressing LRRTM4-CFP but not to control cells expressing CFP or the unrelated synaptogenic protein netrin G ligand 3 (NGL-3)-CFP. Binding of Myc-GPC5-AP to cells expressing HA-LRRTM4 was saturable and Scatchard analysis yielded an estimated apparent dissociation constant (k_D) of 24.3 nM. This value is in the same range as the apparent k_D for binding of neurexin1β-Fc to cell surface-expressed HA-LRRTM2 and HA-neuroligin-1 (9.6 to 26.9 nM) as assessed in a similar assay (Siddiqui et al., 2010), suggesting that this interaction is of physiological relevance. Thus, LRRTM4 binds with high affinity to glypicans and syndecans via their HS chains.

In *trans* Recruitment of Axonal HSPGs by LRRTM4 and of Dendritic LRRTM4 by HSPGs to Cell Contact Sites

To determine whether LRRTM4 and HSPGs interact in *trans* on cellular surfaces and recruit each other to developing contact sites, we cocultured COS7 cells expressing LRRTM4 with neurons expressing HSPGs and vice versa. LRRTM4-CFP expressed in COS7 cells was able to recruit neuronally expressed HA-GPC5 or HA-SDC2 but not HA-GPC5ΔGAG to contact sites (Figures 3A and 3B). HA-GPC5 targeted selectively to axons in cultured hippocampal neurons, both in pure neuron cultures and in the COS7 cocultures (Figure S3). HA-SDC2 targeted to both axons and dendrites, although LRRTM4-expressing COS7 cells induced local aggregation of both recombinant HSPGs mainly along contacting axons in coculture. This result indicates that LRRTM4 on dendrites could recruit axonal HSPGs to contact sites. Conversely, Myc-GPC5 or Myc-SDC2 but not Myc-GPC5ΔGAG expressed in COS7 cells could recruit neuronally expressed mCherry-LRRTM4 to contact sites (Figures 3C and 3D). Consistent with the somatodendritic targeting of recombinant LRRTM4 in pure neuron cultures (Figure 1), HSPG-expressing COS7 cells induced local aggregation of recombinant LRRTM4 along contacting dendrites but not axons in coculture. This result indicates that HSPGs on axons could recruit dendritic LRRTM4 to contact sites. The absence of recruitment activity by Myc-GPC5ΔGAG indicates that the HS chains are required for the mutual recruitment of LRRTM4 and HSPGs to cell contact sites.

Axonal HSPGs Are Essential for Presynaptic Differentiation Induced by LRRTM4

To assess the role of the LRRTM4-HSPG interaction in synaptic development, we built on our finding that heparinase-mediated cleavage of the HS chains of glypicans and syndecans disrupts their interaction with LRRTM4-Fc in the cell-based binding assay (Figure 2). If the LRRTM4-HSPG interaction is necessary for the ability of neuronally overexpressed LRRTM4 to increase presynaptic inputs, heparinase cotreatment should block the effects of neuronal overexpression of LRRTM4 on presynaptic inputs. Indeed, using two distinct markers for presynaptic inputs, the active zone protein bassoon and the vesicle-associated protein synapsin, we found that overexpression of YFP-LRRTM4 in cultured neurons increased immunofluorescence for presynaptic markers onto expressing dendrites and that this effect was abolished by cotreatment with heparinases (Figures 4A and 4B). To test the specificity of the effects of heparinases, we did parallel experiments with another synaptogenic protein NGL-3 (Woo et al., 2009), which we found to be of similar potency as LRRTM4. Overexpression of NGL-3-CFP in cultured neurons induced a very similar increase in immunoreactivity for presynaptic bassoon and synapsin along transfected dendrites as did overexpression of YFP-LRRTM4, yet these effects of NGL-3 were resistant to heparinase treatment (Figures 4A and 4B). This control experiment rules out potential nonspecific effects of the heparinase treatment on cell health and ability to develop synapses. Thus, HSPGs are required specifically for LRRTM4 to enhance presynaptic differentiation.

In this neuron overexpression experiment (Figure 4), HSPGs on axons, on dendrites, or in the form of cleaved ectodomains could potentially be acting in concert with LRRTM4 to enhance presynaptic differentiation, although the COS7 cell-neuron recruitment assays (Figure 3) indicate that the axonal HSPGs may be most important. To further differentiate among these possibilities, we used a coculture presynapse induction assay following methods used previously to demonstrate synaptogenic activity of neuroligins and LRRTMs (Linhoff et al., 2009; Scheiffele et al., 2000). Consistent with these previous results, Myc-LRRTM4 expressed on COS7 cells induced clustering of bassoon along contacting axons of cocultured hippocampal neurons (Figures 5A and 5B). This presynapse-inducing activity of LRRTM4 was abolished by cotreatment with heparinases, whereas the presynapse induction by NGL-3-CFP was unaffected by heparinases. Furthermore, pretreatment of neuron-COS7 cell cocultures with heparinases followed by growth in glial-conditioned medium over glial feeder layers lacking heparinases also abolished the presynapse-inducing activity of Myc-LRRTM4 but not that of NGL-3-CFP (Figure 5B, right). Thus, the source of required HSPGs is the neurons or COS7 cells

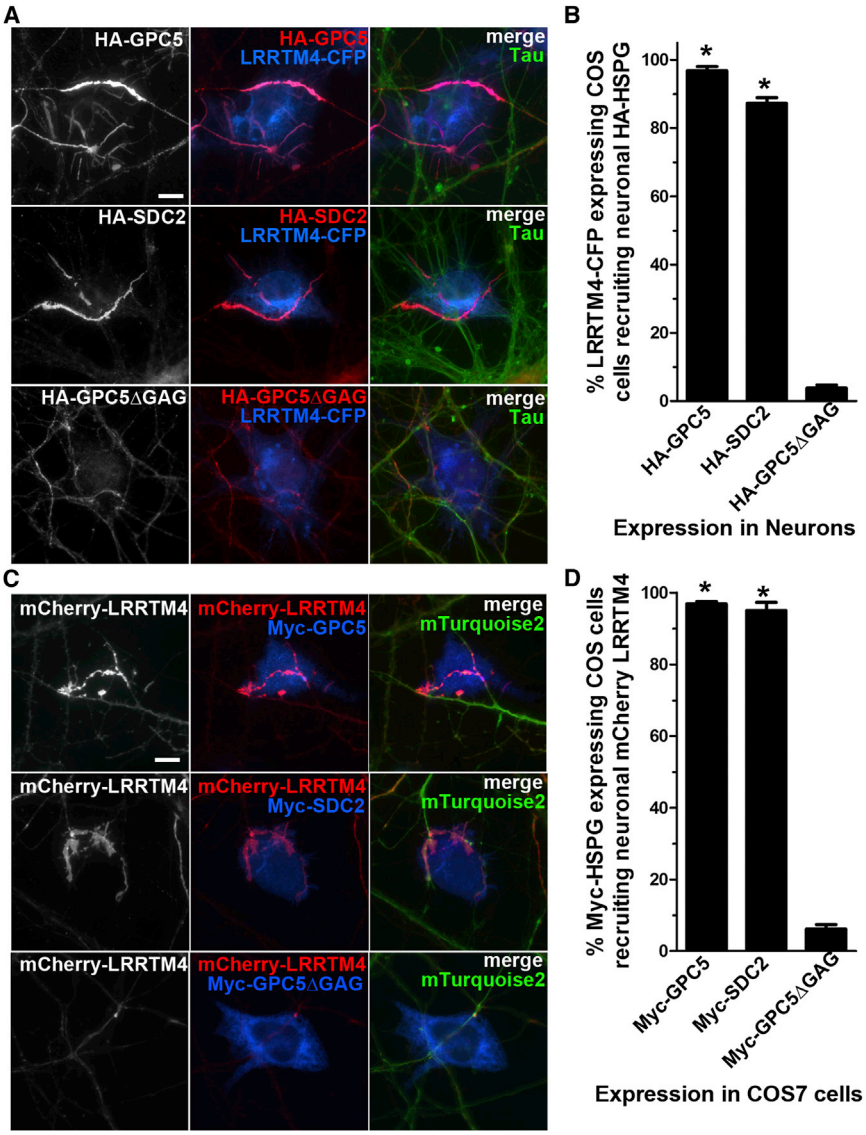

Figure 3. LRRTM4 In *trans* Recruits Axonal HSPGs, and HSPGs In *trans* Recruit Dendritic LRRTM4, to Cell Contact Sites

(A) Cultured hippocampal neurons were transfected at plating to express the indicated HA-tagged glypican (GPC) or syndecan (SDC) and were cocultured at 11 DIV with COS7 cells expressing LRRTM4-CFP. LRRTM4-CFP on COS7 cells recruited HA-GPC5 and HA-SDC2, but not the HS-deficient mutant HA-GPC5ΔGAG, to high local density at cell contact sites along dephospho-tau-positive axons.

(B) Quantitation of the percentage of COS7 cells expressing LRRM4-CFP and in contact with HA-HSPG-expressing axons that induced local recruitment of the HA-HSPG. ANOVA $p < 0.0001$, *$p < 0.001$ compared with HA-GPC5ΔGAG by Tukey's multiple comparison test, n = 3 experiments.

(C) Cultured neurons were transfected at plating to coexpress mCherry-LRRTM4 and mTurquoise cell fill and were cocultured at 11 DIV with COS7 cells expressing the indicated Myc-tagged GPC or SDC. Myc-GPC5 and Myc-SDC2, but not the HS-deficient mutant Myc-GPC5ΔGAG, on COS7 cells recruited mCherry-LRRTM4 but not mTurquoise to high local density at cell contact sites along dendrites.

(D) Quantitation of the percentage of COS7 cells expressing the indicated Myc-HSPG and in contact with mCherry-LRRTM4-expressing dendrites that induced local recruitment of mCherry-LRRM4. ANOVA $p < 0.0001$, *$p < 0.001$ compared with Myc-GPC5ΔGAG by Tukey's multiple comparison test, n = 2–3 experiments.

Data are presented as mean ± SEM. Scale bars represent 10 μm.

See also Figure S3.

and not the glia cells. To assess a potential contribution of HSPGs from the COS7 cells, we next performed neuron coculture assays with gro2C cells, an L cell-derived line that is specifically defective in the HS synthesis pathway (Gruenheid et al., 1993). These HS-lacking gro2C cells were as effective as the parent L cells in allowing expressed LRRTM4-CFP to induce synapsin clustering in contacting axons of cocultured neurons (Figures 5C and 5D). Thus, HSPGs are required in the contacting neurons for presynapse induction by LRRTM4.

To further assess the role of soluble HSPG ectodomains in presynapse induction by LRRTM4, we added recombinant glypican ectodomain fused with alkaline phosphatase (glypican-AP) during the coculture assay. Glypican-AP as compared with control AP significantly reduced synapsin clustering in axons contacting HA-LRRTM4-expressing COS7 cells (Figures 5E and 5F). In the same assay, glypican-AP did not affect synapsin clustering in axons contacting NGL-3-CFP-expressing COS7 cells. This selective reduction in synaptogenic activity of LRRTM4 by glypican-AP provides independent evidence from the heparinase experiments that HSPGs mediate presynaptic induction by LRRTM4. Furthermore, taken together, these coculture results indicate that HSPGs are required in the contacting axons to mediate presynaptic differentiation induced by LRRTM4 and that soluble HSPGs from glia are not required and may even have suppressive effects.

LRRTM4$^{-/-}$ Mice Are Deficient in Excitatory Synapse Development on Dentate Gyrus Granule Cells

To genetically perturb the function of the LRRTM4-HSPG complex in mice in vivo, we focused on LRRTM4 because multiple proteoglycans can interact with LRRTM4 and we expect that deletion of multiple proteoglycans would be required to perturb the function of LRRTM4-HSPG signaling. We generated mice with a targeted deletion in *LRRTM4* by deleting exon 2, which encodes a large portion of the LRRTM4 protein (Figures S4A). Loss of LRRTM4 protein was confirmed by western blot analysis of whole mouse brain homogenate (Figure 6A) and by confocal

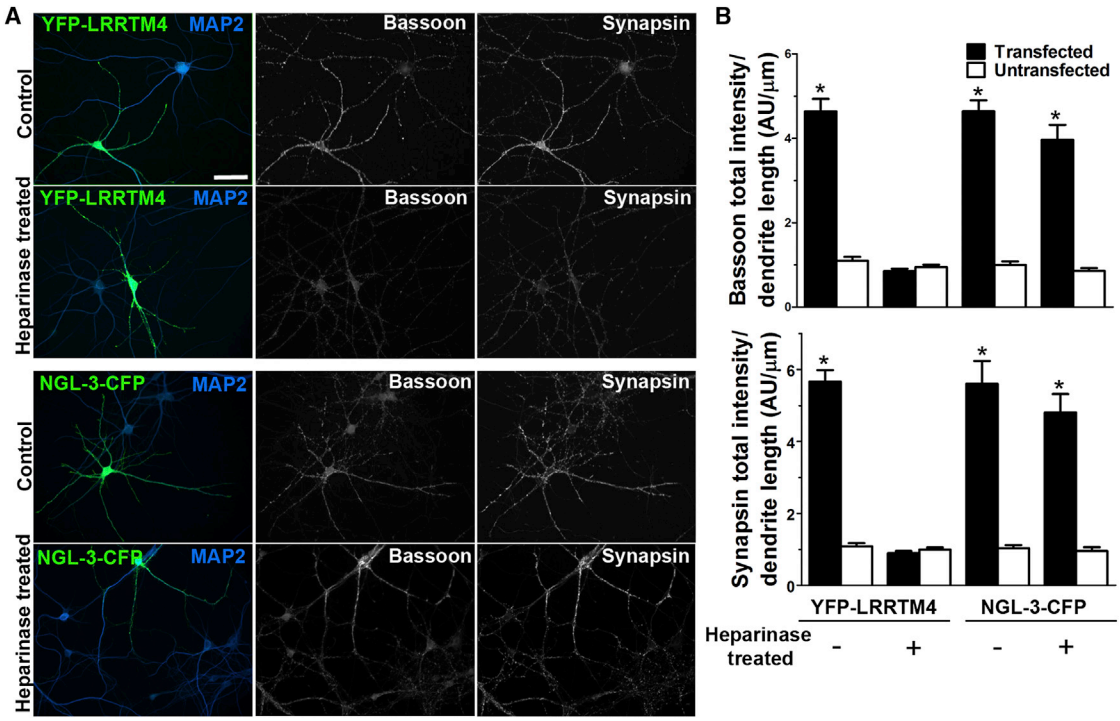

Figure 4. HSPGs Are Required for Enhancement of Presynaptic Inputs by Overexpression of LRRTM4

(A) Cultured hippocampal neurons were transfected at 9–10 DIV with YFP-LRRTM4 or NGL-3-CFP and then grown for 20–24 hr in the presence or absence of heparinases to cleave the HS chains of HSPGs. Overexpression of either YFP-LRRTM4 or NGL-3-CFP resulted in increased immunofluorescence for the presynaptic markers bassoon and synapsin along transfected dendrites as compared with neighboring untransfected neurons (similar to Figure S1). Heparinase treatment blocked the effect of YFP-LRRTM4 but not of NGL-3-CFP on presynaptic inputs.

(B) Quantitation of the integrated intensity of bassoon or synapsin puncta per dendrite length. ANOVA $p < 0.0001$, $^*p < 0.001$ comparing each transfected group with the associated untransfected group by Tukey's multiple comparison test, n = 21 cells each.

Data are presented as mean ± SEM. Scale bar represents 50 μm.

microscopy analysis of brain sections with an anti-LRRTM4 antibody (Figure 6B). *LRRTM4*$^{-/-}$ mice were viable and fertile and indistinguishable from wild-type mice with respect to gross brain morphology and cytoarchitectural organization as assessed by confocal microscopy analysis of brain sections labeled for the nuclear marker DAPI, the synaptic marker synapsin, the dendritic marker MAP2, and the axonal marker dephospho-tau (Figures 6B and 6C and data not shown).

Given the high levels of LRRTM4 in the molecular layers of dentate gyrus, we tested whether levels of HSPGs and key postsynaptic molecules may be altered in the dentate gyrus of *LRRTM4*$^{-/-}$ mice. We prepared crude synaptosomal fractions from isolated dentate gyri from *LRRTM4*$^{-/-}$ and control wild-type mice at 6–7 weeks postnatally, a time when LRRTM4 expression reaches a plateau (Figure 1A). Quantitative immunoblotting of these fractions revealed no difference between *LRRTM4*$^{-/-}$ and wild-type mice in the level of AMPA receptor subunits GluA1 and GluA2 (Figures 6D and 6E). While the level of the inhibitory synapse scaffolding molecule gephyrin remained unchanged, the level of PSD-95 family proteins was significantly reduced in *LRRTM4*$^{-/-}$ mice, indicating that LRRTM4 is an important component of excitatory postsynapses in the dentate gyrus. Next, we determined whether the level of HSPGs may be affected by the loss of LRRTM4. Representatives of glypicans and syndecans, GPC2 and SDC4 were both significantly reduced in the crude synaptosomal fractions of *LRRTM4*$^{-/-}$ mice dentate gyri. Moreover, using an antibody that recognizes the glycosaminoglycan stub region after heparinase treatment, we found that the total level of all HSPGs in crude synaptosomal fractions of *LRRTM4*$^{-/-}$ mice dentate gyri was significantly reduced, indicating that LRRTM4 is an important functional partner of HSPGs.

We next performed confocal imaging of excitatory and inhibitory synaptic markers in *LRRTM4*$^{-/-}$ dentate gyrus molecular layers, in comparison with CA1 stratum oriens, a region where LRRTM4 is not expressed (Figures 1 and 6; Laurén et al., 2003; Lein et al., 2007), again at 6–7 weeks postnatally. Quantitative confocal analysis revealed reduced punctate VGlut1 immunofluorescence in all dentate gyrus molecular layer regions but not in CA1 stratum oriens in *LRRTM4*$^{-/-}$ mice as compared with wild-type littermates (Figures 6F and 6G). In contrast, punctate immunofluorescence of the GABA synthetic enzyme glutamic acid decarboxylase GAD65 in the same colabeled regions was indistinguishable between *LRRTM4*$^{-/-}$ and wild-type littermate mice (Figures 6H and 6I). Thus, LRRTM4 is required for the development of excitatory presynapses in specific brain regions.

The vast majority of excitatory synapses on dentate gyrus granule cells and CA1 pyramidal neurons form on dendritic spines (Harris and Kater, 1994; Trommald and Hulleberg, 1997). Thus, we counted spine density in Golgi-stained brain sections. Spine density on dentate gyrus granule cell dendrites in the outer molecular layer (the region receiving inputs from the medial entorhinal cortex) was significantly reduced in *LRRTM4*$^{-/-}$ mice as compared with wild-type littermates, while CA1 pyramidal neuron dendrites in stratum oriens showed no difference (Figures 7A and 7B). To rule out any potential artifacts caused by the slow fixation in Golgi-stained tissue, we also confirmed the reduction in spine density in the dentate gyrus of *LRRTM4*$^{-/-}$ mice by carbocyanine dye dil labeling of perfused tissue (Figure S5).

These data indicate that excitatory synapse density is selectively reduced in dentate gyrus granule cells of *LRRTM4*$^{-/-}$ mice. To further characterize this phenotype, we assessed immunofluorescence for synaptic markers in primary hippocampal neurons after 2 weeks in low-density culture, a system in which synaptic protein clusters can be clearly resolved. We used the high level of calbindin immunofluorescence (Westerink et al., 2012) and the distinct dendritic morphology to identify dentate gyrus granule cells in primary culture (Figure 7C). A reduced density of PSD-95-positive VGlut1 clusters was found specifically in dentate gyrus granule cells but not in pyramidal cells of *LRRTM4*$^{-/-}$ neurons as compared with wild-type littermate neurons (Figures 7D and 7E). Altogether, these data lead us to conclude that LRRTM4 promotes formation of excitatory synapses on hippocampal dentate gyrus granule cells but not on pyramidal cells.

LRRTM4 Contributes to Activity-Regulated Synaptic Insertion of AMPA Receptors

Given the association of LRRTM4 with AMPA receptors (Figure 1C; Schwenk et al., 2012), we next used the dissociated neuron culture system to assess effects of LRRTM4 loss on synaptic surface levels of AMPA receptors containing GluA1 (Figures 7F and 7G). We measured the average GluA1 surface immunofluorescence at postsynaptic sites identified by PSD-95 cluster area, thus reflecting the average intensity of surface GluA1 per postsynapse. *LRRTM4*$^{-/-}$ dentate gyrus granule cells showed no difference in basal levels of surface GluA1 per synapse compared with dentate gyrus granule cells from littermate wild-type mice. AMPA receptors undergo activity-regulated trafficking, a process that contributes to many forms of synaptic plasticity (Anggono and Huganir, 2012; Malinow and Malenka, 2002). Thus, we tested the role of LRRTM4 in synaptic insertion of GluA1 in response to a chemical stimulation protocol that involves selective activation of synaptic NMDA receptors and results in long-term potentiation (LTP) in cultured hippocampal neurons (Lu et al., 2001). Whereas wild-type dentate gyrus granule cells showed a significant increase in synaptic immunofluorescence for surface GluA1 after the chemical LTP induction protocol, *LRRTM4*$^{-/-}$ dentate granule showed only a small increase that did not constitute a significant difference as compared with unstimulated cells. Thus, LRRTM4 not only controls excitatory synapse development but also contributes to activity-regulated synaptic insertion of surface AMPA receptors in dentate gyrus granule cells.

Excitatory Transmission Is Impaired in *LRRTM4*$^{-/-}$ Dentate Gyrus Granule Cells

To test for changes in excitatory synapse function as a consequence of loss of LRRTM4, we performed whole-cell recordings from dentate gyrus granule cells in hippocampal slices of *LRRTM4*$^{-/-}$ and wild-type littermate mice (Figure 8). Miniature excitatory postsynaptic current (mEPSC) recordings from *LRRTM4*$^{-/-}$ neurons revealed a 35% reduction in mEPSC frequency as compared to wild-type control neurons (corresponding to an increased interevent interval, Figure 8B). No significant difference in mEPSC amplitude was detected (Figure 8C). To determine whether changes in mEPSC frequency were specific to dentate gyrus granule cells, we recorded mEPSCs in CA1 pyramidal cells. No significant difference in mEPSC frequency (Figure 8E) or amplitude (Figure 8F) was detected between *LRRTM4*$^{-/-}$ and wild-type littermate CA1 neurons. Thus, LRRTM4 contributes to development of functional excitatory synapses selectively in dentate gyrus granule neurons. The observed reduction in mEPSC frequency but not amplitude is consistent with the imaging data, indicating a role for LRRTM4 in controlling excitatory synapse density specifically on dentate gyrus granule neurons.

We next assessed inhibitory synapse function but found no difference in frequency or amplitude of miniature inhibitory postsynaptic currents (mIPSCs) in dentate gyrus granule cells in slices of *LRRTM4*$^{-/-}$ mice as compared with wild-type mice (Figure S5). Based on the reduction in excitatory but not inhibitory spontaneous currents, we expected evoked transmission to be reduced in the absence of LRRTM4. To test this prediction, input/output curves were generated by stimulating perforant pathway fibers while recording field excitatory postsynaptic potential (fEPSP) responses from the dentate gyrus molecular layer. Indeed, fEPSP slope was significantly reduced in *LRRTM4*$^{-/-}$ as compared with wild-type slices (Figures 8F and 8G), indicating reduced evoked transmission. In contrast, paired-pulse ratio at these synapses showed no difference between genotypes (Figure 8H), suggesting that LRRTM4 does not affect release probability, which is again consistent with a reduction in synapse number in *LRRTM4*$^{-/-}$ dentate gyrus.

DISCUSSION

We show using overexpression and genetic knockout approaches that LRRTM4 promotes excitatory synapse development. LRRTM4 is highly expressed by dentate gyrus granule cells, is localized at excitatory postsynaptic sites in all dendritic laminae, and associates with excitatory postsynaptic scaffold proteins of the PSD-95 family and AMPA receptors. In *LRRTM4*$^{-/-}$ mice, dentate gyrus granule cells but not CA1 neurons show reductions in VGlut1 but not GAD65 immunoreactive inputs and in spine density. *LRRTM4*$^{-/-}$ dentate gyrus granule cells in primary culture show deficits in excitatory synapse density and in activity-induced synaptic recruitment of AMPA receptors. Moreover, loss of LRRTM4 causes a deficit in excitatory synaptic transmission specifically in dentate gyrus granule cells and not CA1 pyramidal neurons in acute brain slice. Loss of LRRTM4 also results in a reduced level of PSD-95 family proteins in dentate gyrus crude synaptosomes. Thus, LRRTM4

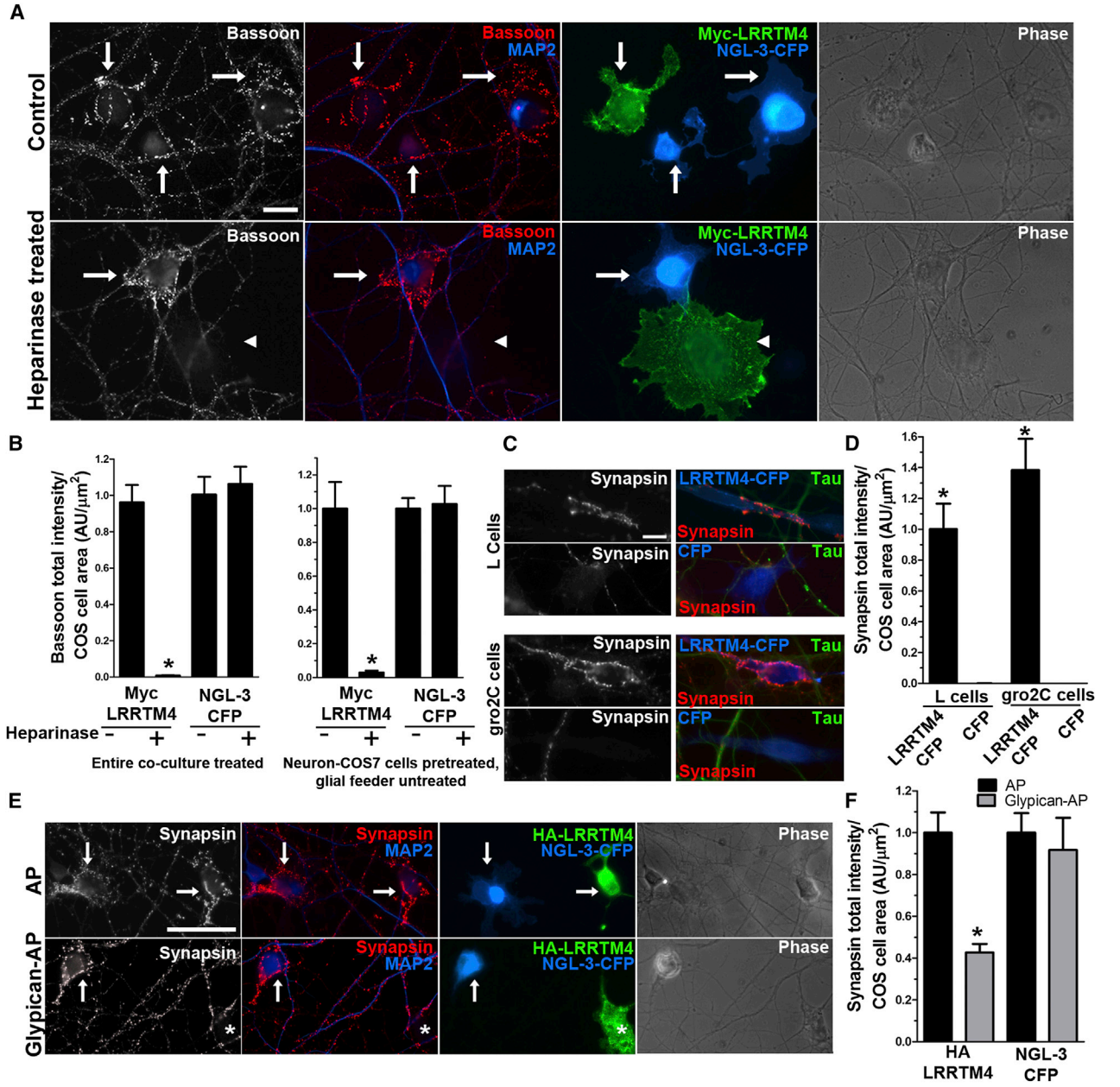

Figure 5. Axonal HSPGs Are Required for Presynaptic Induction by LRRTM4 in a Coculture Assay

(A) COS7 cells expressing Myc-LRRTM4 or NGL-3-CFP and cocultured with hippocampal neurons at 13 DIV induced clustering of bassoon in contacting axons at sites lacking MAP2-positive dendrite contact (arrows). Heparinase treatment during the coculture period blocked presynaptic induction by Myc-LRRTM4 (arrowhead) indicating a requirement for HSPGs, whereas NGL-3-CFP synaptogenic activity was not affected by heparinases (arrow).

(B) Quantitation of the integrated intensity of bassoon immunofluorescence associated with COS7 cells expressing the indicated construct and not associated with MAP2 when heparinases were included during the coculture period (left) or when neuron-COS7 cell cocultures were pretreated with heparinases and then grown with an untreated glial feeder layer (right). ANOVA $p < 0.0001$, $^*p < 0.001$ comparing conditions with or without heparinase treatment for each construct by Tukey's multiple comparison test, n = 29 cells each (left) or 13–16 cells each (right).

(C) Similar to the parental L cells, HS-deficient gro2C cells expressing LRRTM4-CFP but not CFP control induced clustering of synapsin in contacting dephospho-tau-positive axons of cocultured hippocampal neurons at sites lacking MAP2-positive dendrites (MAP2 not shown).

(D) Quantitation of the integrated intensity of synapsin immunofluorescence associated with L cells or gro2C cells expressing the indicated construct and not associated with MAP2. ANOVA $p < 0.0001$, $^*p < 0.001$ comparing LRRTM4-CFP with CFP for each cell line by Tukey's multiple comparison test, $p > 0.05$ comparing L cells with gro2C cells for LRRM4-CFP, n = 8–15 cells each.

(E) COS7 cells expressing HA-LRRTM4 or NGL-3-CFP and cocultured with hippocampal neurons at DIV14 in the presence of recombinant AP protein induced clustering of synapsin in contacting axons at sites lacking MAP2-positive dendrites (arrows). Application of a mix of recombinant glypican4-AP and glypican5-AP during the coculture period reduced presynaptic induction by HA-LRRTM4 (asterisk) but not by NGL-3-CFP (arrow).

(legend continued on next page)

contributes to excitatory presynapse and postsynapse development. Further, we identify a new family of LRRTM4 ligands, HSPGs, thus differentiating LRRTM4 from LRRTM1 and LRRTM2, which bind the LNS domain of neurexins. LRRTM4 can directly bind to multiple glypicans and syndecans, and their interaction requires the HS chains. Furthermore, HSPGs are required for presynaptic differentiation induced by LRRTM4, and levels of HSPGs are reduced in the dentate gyrus of *LRRTM4*$^{-/-}$ mice. Thus, different postsynaptic LRRTM family members function in synapse organization through different presynaptic mechanisms, and the LRRTM4-HSPG complex is particularly important for proper development of glutamatergic synapses on dentate gyrus granule cells.

HSPGs have previously been implicated in synapse development and function (Van Vactor et al., 2006; Yamaguchi, 2001). Agrin is a well-known synapse-organizing protein at the mammalian neuromuscular junction (Wu et al., 2010), and syndecan and the glypican Dally-like regulate synapse development in different ways at the *Drosophila* neuromuscular junction (Johnson et al., 2006). However, the mechanisms of action of HSPGs at central synapses are less well understood. The major HSPGs in the brain are the cell surface GPI-anchored glypicans, the transmembrane syndecans, and the secreted proteins agrin and perlecan. Syndecan-2 is present at both presynaptic and postsynaptic sites of glutamatergic synapses (Hsueh et al., 1998), and postsynaptic syndecan-2 regulates dendritic spine development (Ethell et al., 2001). Glypican-4 and glypican-6 released from glia cells after phospholipase cleavage were recently shown to promote GluA1-containing AMPA receptor surface insertion and functional synapse development in isolated retinal ganglion cells (Allen et al., 2012). All glypicans are expressed by neurons, thus neuronal glypicans in their cell surface GPI-anchored or cleaved soluble forms may also contribute to synapse development. Exostosin Ext1 is an essential enzyme for the synthesis of the HS chains of HSPGs, and conditional knockout of *EXT1* in late postnatal neurons causes deficits in excitatory synaptic transmission and a reduction in surface AMPA receptors (Irie et al., 2012). Acute cleavage of HS chains does not alter basal transmission in hippocampal slices but prevents long-term potentiation (Lauri et al., 1999). Thus, several studies link HSPGs to postsynapse maturation and plasticity.

In contrast to their role in postsynapse maturation, a function of HSPGs in central neuron presynapse maturation has so far not been described, although HSPGs were found to be essential for the induction of axonal synaptic vesicle clusters by artificial cationic beads (Lucido et al., 2009). Our findings show that HSPGs are essential mediators of presynapse induction via their interaction with the native synapse-organizing protein LRRTM4. Axonal surface HSPGs were recruited by and are necessary for presynapse induction by LRRTM4 (Figures 3, 4, and 5).

LRRTM4 directly binds to all HSPGs tested (Figure 2). The interaction of LRRTM4 with HSPGs requires the HS chains and appears to be relatively independent of the glypican or syndecan backbone. Further studies will be required to determine whether specific glypicans or syndecans or other HSPGs mediate presynapse induction by LRRTM4, and what downstream mechanisms are involved. Among the glypicans (1, 3, 4, and 5) that were affinity purified on the LRRTM4-Fc matrix, glypican-1 and glypican-5 are highly expressed by entorhinal cortex inputs to dentate gyrus granule cells (Ohmi et al., 2011). If the GPI-linked glypicans act as the functional axonal receptors through which LRRTM4 induces presynaptic differentiation, their lack of intracellular domains predicts the necessity of additional axonal surface proteins that interact with glypicans to transduce the synapse-organizing signal.

Our findings also raise interesting possibilities for modulation of LRRTM4 function by soluble or postsynaptic HSPGs. The inhibitory effect of soluble recombinant glypican-AP (Figures 5E and 5F) suggests that native glypican and syndecan ectodomains shed from neurons and glia might inhibit the interaction of LRRTM4 with cell-surface HPSGs and act as negative regulators of LRRTM4-mediated synapse development. Other secreted HSPGs such as agrin and perlecan may have similar negative regulatory roles, unless they can bridge presynaptic and postsynaptic sites through additional partners. Dendritic syndecans might also interact with LRRTM4 in *cis* at postsynaptic sites, with consequences more difficult to predict.

The reductions in spine density and in VGlut1 input puncta immunofluorescence in *LRRTM4*$^{-/-}$ dentate gyrus granule cells in vivo and the reduced density of PSD-95-positive VGlut1 clusters in cultured *LRRTM4*$^{-/-}$ dentate gyrus granule cells (Figures 6 and 7) indicate that loss of LRRTM4 results in a reduction in excitatory synapse density in the dentate gyrus. A corresponding functional reduction in excitatory synaptic transmission is indicated by the reductions in evoked transmission and in mEPSC frequency in *LRRTM4*$^{-/-}$ dentate gyrus granule cells (Figure 8). The absence of any effect of the LRRTM4 loss on mEPSC amplitude parallels the normal basal levels of surface GluA1 found at the remaining synapses of dentate gyrus granule cells cultured from the *LRRTM4*$^{-/-}$ mice.

The reduction in activity-induced synaptic recruitment of GluA1 in the absence of LRRTM4 indicates additional roles for the LRRTM4-HSPG complex in postsynaptic plasticity. It is tempting to speculate that the observed reduction in PSD-95 family proteins (Figures 6D and 6E), which have been intensively studied for their roles in regulating AMPA receptor function and trafficking in other systems (Elias et al., 2008; Xu, 2011), may mediate this change in regulated AMPA receptor trafficking upon loss of LRRTM4. Consistent with our data (Figure 1C), LRRTM4 was recently isolated as one of about two dozen proteins that copurify with native AMPA receptors (Schwenk et al., 2012). Among these, LRRTM4 was not a stable core component of AMPA receptor complexes, but rather the association with AMPA receptors was dependent upon the assay conditions. Such labile association is consistent with a role of LRRTM4 in

(F) Quantitation of the integrated intensity of synapsin immunofluorescence associated with COS7 cells expressing the indicated construct and not associated with MAP2. ANOVA $p = 0.0002$, $^{*}p < 0.001$ comparing cocultures in the presence of AP and glypican-AP for each construct by Tukey's multiple comparison test, $n = 19–20$ cells each.

Data are presented as mean ± SEM. Scale bars represent 20 μm in (A) and 10 μm in (C) and (E).

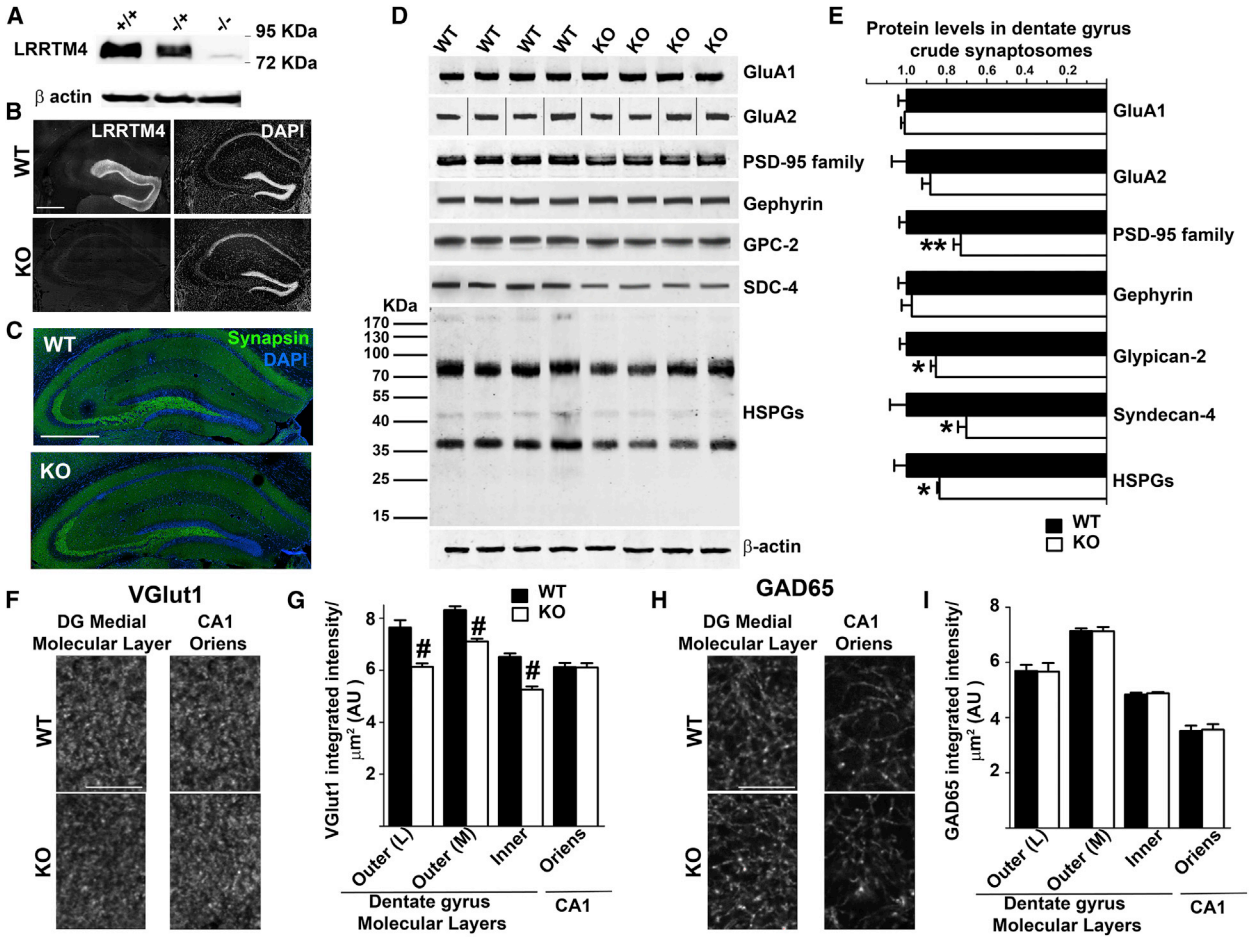

Figure 6. *LRRTM4*$^{-/-}$ Mice Show Altered Molecular Composition and Impaired Excitatory Presynapse Development in Dentate Gyrus

(A) Western blot confirmation of loss of LRRTM4 protein in *LRRTM4*$^{-/-}$ mouse brain homogenate.

(B and C) Immunofluorescence for LRRTM4 confirmed loss of protein in dentate gyrus molecular layers in *LRRTM4*$^{-/-}$ mice. Confocal immunofluorescence images for synapsin and the nuclear marker DAPI revealed normal hippocampal morphology and large-scale synaptic organization in *LRRTM4*$^{-/-}$ (KO) as compared with wild-type (WT) mice.

(D) Western blotting of crude synaptosomal fractions from dentate gyrus of 6- to 7-week-old *LRRTM4*$^{-/-}$ and wild-type control mice reveal that excitatory postsynaptic scaffolding PSD-95 family molecules (using an antibody that recognizes PSD-95, PSD-93, SAP102, and SAP97) but not inhibitory scaffolding molecule gephyrin are reduced in *LRRTM4*$^{-/-}$ mice. Overall HSPGs revealed with an antibody against the glycosaminoglycan stub region after heparinase treatment, as well as the glypican GPC2 and syndecan SDC4, are also reduced in *LRRTM4*$^{-/-}$ mice.

(E) Quantitation of western blots in (D), normalized to β-actin loading controls. *$p < 0.05$, **$p < 0.01$, t test, n = 4 mice per genotype.

(F and H) High-resolution confocal images revealed a reduction in punctate immunofluorescence for VGlut1 in the dentate gyrus molecular layer but not in CA1 stratum oriens in *LRRTM4*$^{-/-}$ mice as compared with wild-type at 6 weeks postnatal. No difference was observed in the inhibitory presynapse marker GAD65 by double labeling of the same regions.

(G and I) Quantitation of VGlut1 and GAD65 punctate integrated intensity per tissue area. Within the dentate gyrus outer molecular layer, L and M indicate the more distal or proximal regions that receive inputs from the later or medial entorhinal cortex, respectively. ANOVA $p < 0.0001$, #$p < 0.001$ comparing *LRRTM4*$^{-/-}$ and littermate wild-type mice for each region by Tukey's multiple comparison test, n = 5–6 mice each after averaging data from 6 sections per mouse.

Data are presented as mean ± SEM. Scale bars represent 500 μm in (B) and (C) and 10 μm in (F) and (H).

the activity-regulated recruitment of AMPA receptors to synapses as indicated by our data.

All our evidence indicates a role for LRRTM4 exclusively at excitatory postsynaptic sites in a cell-type-specific manner. LRRTM4 promotes only excitatory and not inhibitory presynapse differentiation both in coculture assays (Linhoff et al., 2009) and upon overexpression in neurons (Figure S1). YFP-LRRTM4 expressed in cultured neurons localizes exclusively to excitatory postsynaptic sites, and we observed very high levels of LRRTM4 protein at excitatory postsynaptic sites throughout the dentate gyrus inner and outer molecular layers (Figure 1). LRRTM4 was not detected in the mossy fiber axonal output region of dentate gyrus granule cells. The abundance of LRRTM4 in dentate gyrus molecular layers is consistent with the high-level expression of LRRTM4 mRNA by dentate gyrus granule cells (Laurén et al., 2003; Lein et al., 2007). Furthermore, and consistent with the expression of LRRTM4 by dentate gyrus granule cells but not CA1 neurons, we found

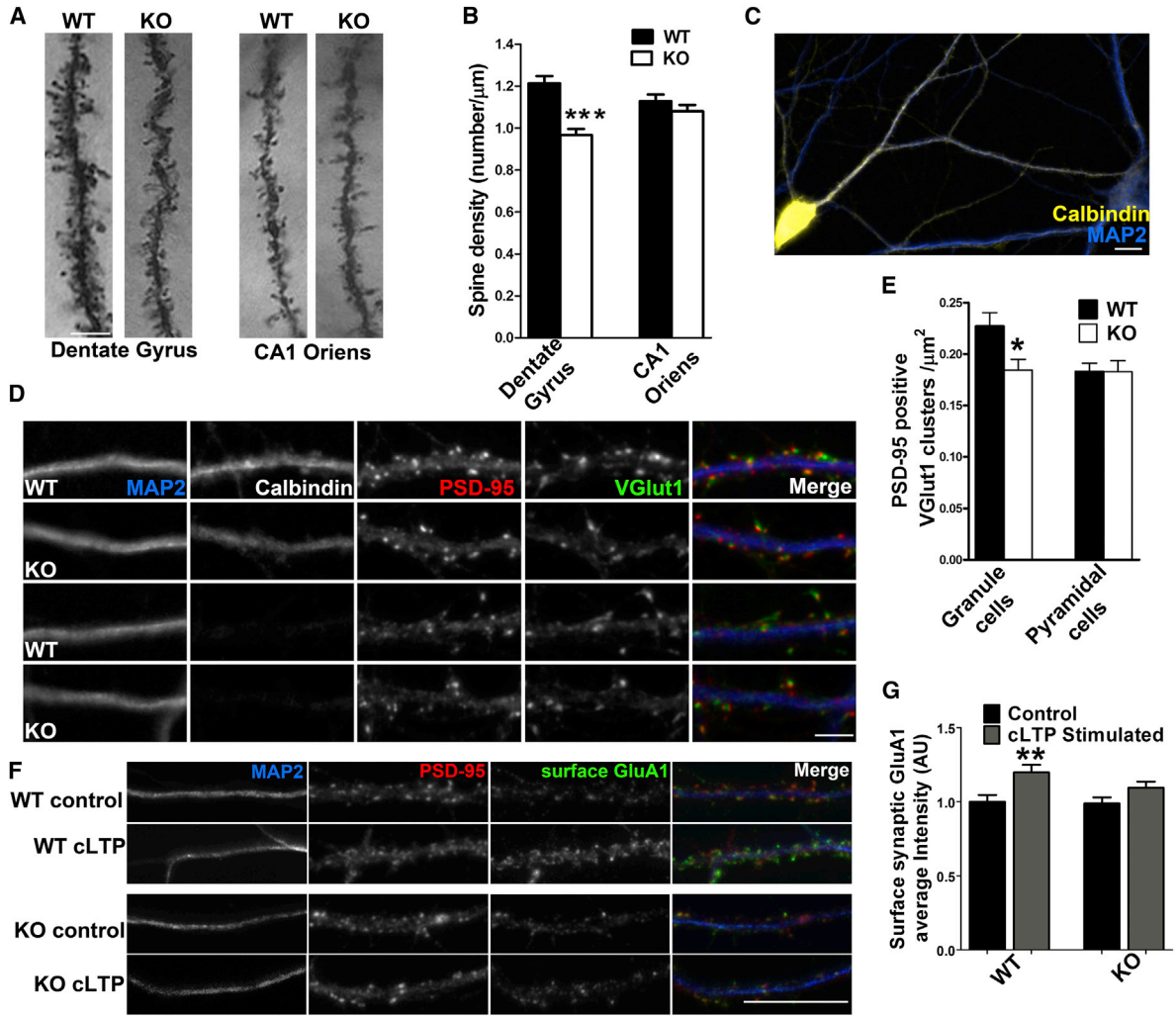

Figure 7. LRRTM4 Contributes to Excitatory Postsynapse Development and AMPA Receptor Trafficking in Dentate Gyrus Granule Cells

(A) Golgi staining revealed a reduced density of dendritic spines along dentate granule cells in the outer molecular layer in *LRRTM4*$^{-/-}$ (KO) mice as compared with wild-type (WT) mice at 6 weeks postnatal. No differences were observed between genotypes along hippocampal CA1 neurons in stratum oriens.

(B) Quantitation of dendritic spine density along dentate granule cell dendrites in the outer molecular layer input region from the medial entorhinal cortex and along CA1 pyramidal cell dendrites in stratum oriens. ***$p < 0.0001$ comparing WT and KO by Student's t test, n = 58–109 dendrites each from 3 mice.

(C–G) In hippocampal neuron cultures prepared from *LRRTM4*$^{-/-}$ and wild-type mice and analyzed at 13–16 DIV, strong calbindin immunoreactivity and distinctive dendritic morphology were used to distinguish dentate granule cells (left cell in C) from pyramidal cells.

(D) *LRRTM4*$^{-/-}$ calbindin-positive dentate granule cell dendrites showed a slight reduction in density of puncta for PSD-95 and VGlut1 as compared with wild-type neurons. No difference between genotypes was observed in calbindin-negative pyramidal cell dendrites.

(E) Quantitation of excitatory synapse density assessed as VGlut1-positive PSD-95 clusters in cultured neurons. *$p < 0.05$ comparing *LRRTM4*$^{-/-}$ and littermate wild-type by Student's t test, n = 40 cells each from 2 independent cultures.

(F) Basal levels of synaptic surface GluA1 on dentate gyrus granule cells identified by morphology and calbindin immunoreactivity (data not shown) did not differ between genotypes. However, a chemical LTP (cLTP) protocol involving selective stimulation of synaptic NMDA receptors induced a greater increase in synaptic surface GluA1 in *LRRTM4*$^{-/-}$ than in littermate wild-type dentate gyrus granule cells.

(G) Quantitation of average intensity of synaptic (defined here as colocalized with PSD-95) surface-labeled GluA1. ANOVA $p < 0.005$, **$p < 0.01$ comparing wild-type control with wild-type cLTP group by Tukey's multiple comparison test ($p > 0.05$ comparing *LRRTM4*$^{-/-}$ control with *LRRTM4*$^{-/-}$ cLTP group, also $p > 0.05$ comparing wild-type control with *LRRTM4*$^{-/-}$ control group), n = 31–34 cells each from 3 independent cultures.

Data are presented as mean ± SEM. Scale bars represent 5 μm in (A) and (D), 10 μm in (C), and 10 μm in (F).

See also Figure S5.

reductions in dendritic spine density and VGlut1 inputs in dentate gyrus molecular layers but not in CA1 stratum oriens of *LRRTM4*$^{-/-}$ mice (Figures 6 and 7). Similarly, only dentate gyrus granule cells showed a reduction in excitatory synapse density in hippocampal cultures from *LRRTM4*$^{-/-}$ mice as compared to wild-type mice. Consistent with the reductions in excitatory synapse density, mEPSC but not mIPSC frequency in *LRRTM4*$^{-/-}$ mice was reduced in dentate gyrus

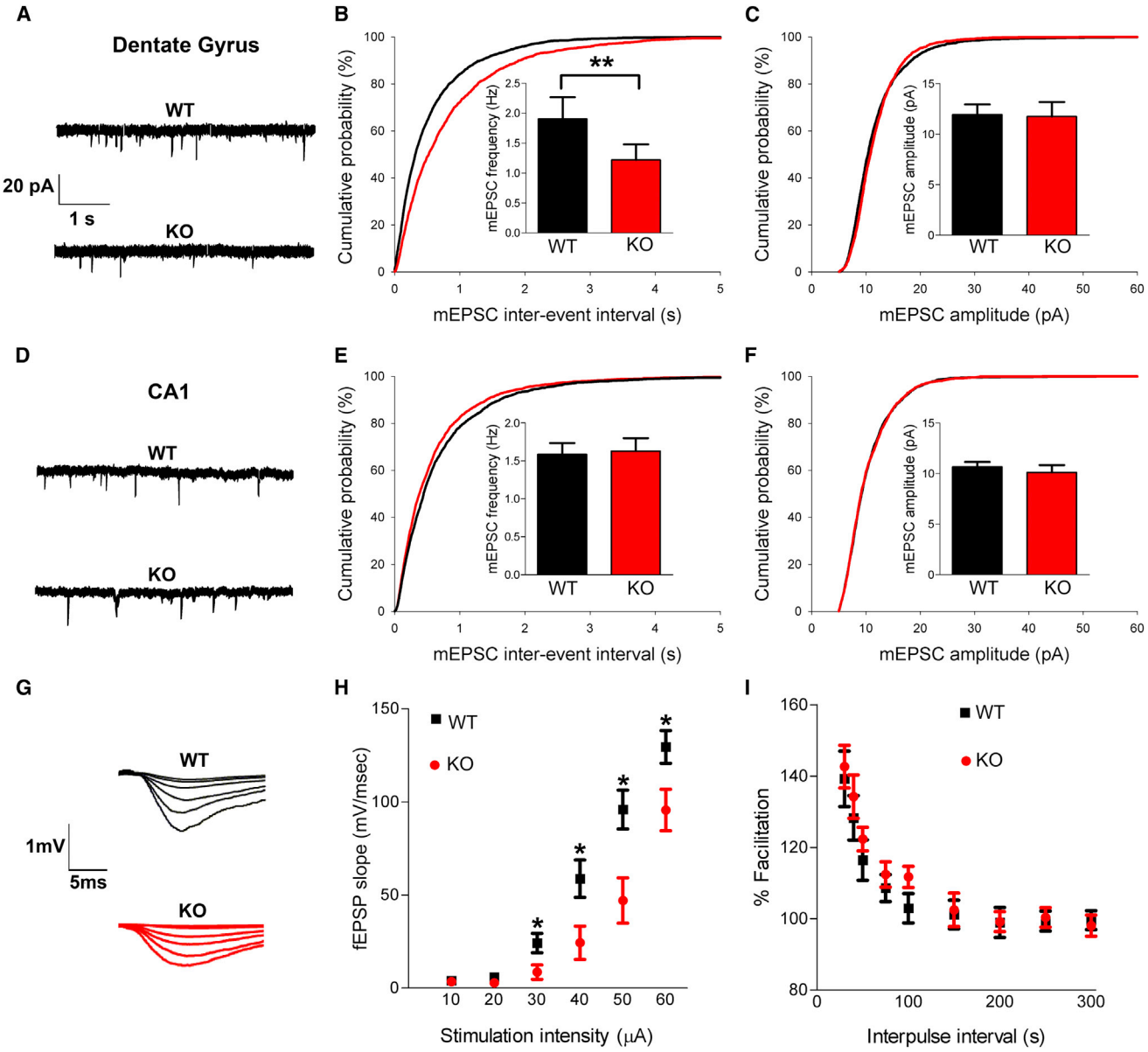

Figure 8. *LRRTM4*$^{-/-}$ Dentate Gyrus Granule Cells Are Deficient in Excitatory Synaptic Transmission

(A) Representative mEPSC recordings from dentate granule cells in acute hippocampal slices from *LRRTM4*$^{-/-}$ (KO) and littermate wild-type (WT) mice.

(B and C) Cumulative distributions of mEPSC interevent intervals (B) and amplitudes (C) in *LRRTM4*$^{-/-}$ and littermate wild-type dentate gyrus granule neurons (wild-type, represented in black; *LRRTM4*$^{-/-}$, represented in red). Insets display mean ± SEM for mEPSC frequency (B) and amplitude (C), respectively. mEPSC frequency was significantly reduced in *LRRTM4*$^{-/-}$ neurons, whereas no differences in amplitude were observed. **$p < 0.01$ by Student's t test, n = 8 cells each.

(D) Representative mEPSC recordings from CA1 pyramidal cells from *LRRTM4*$^{-/-}$ (n = 9) and littermate wild-type (n = 11) hippocampal slices.

(E and F) No significant differences were detected in either mEPSC frequency (E) or amplitude (F) consistent with intact excitatory synaptic transmission in CA1.

(G) Representative fEPSPs from wild-type and *LRRTM4*$^{-/-}$ dentate gyrus in response to increasing stimulation intensity of perforant path inputs.

(H) Input/output curves reveal differences in basal-evoked synaptic responses. fEPSP slope was significantly reduced in *LRRTM4*$^{-/-}$ relative to wild-type slices at higher (>20 μA) stimulation intensities (*$p < 0.05$, t test, n = 10 slices per group).

(I) Paired-pulse facilitation was unchanged in the *LRRTM4*$^{-/-}$ mouse dentate gyrus. Data are presented as mean ± SEM.

See also Figure S6.

granule cells but not in CA1 neurons (Figures 8 and S6). In contrast, LRRTM1 and LRRTM2 contribute to excitatory synapse development on CA1 pyramidal neurons (Soler-Llavina et al., 2011). LRRTM4 is also expressed outside the hippocampus, including in the anterior olfactory nucleus, superficial cortical layers, and striatum. Thus, the LRRTM4-HSPG complex is likely to contribute to synapse development and function in multiple discrete regions.

Like neuroligins, neurexins, and LRRTMs (Francks et al., 2007; Michaelson et al., 2012; Pinto et al., 2010; Südhof, 2008), HSPGs have been linked to cognitive disorders, particularly to autism. Truncating frameshift mutations in *EXT1*, the gene that encodes the essential enzyme for HS biosynthesis, were found in autism patients (Li et al., 2002). Furthermore, a mouse model of late postnatal deletion of *EXT1* in forebrain glutamatergic neurons exhibits impairments in synaptic function along with stereotyped behaviors and deficits in social interaction and ultrasonic vocalization (Irie et al., 2012). Based on this information, we propose that changes in synapse development and synaptic transmission in response to alterations in either LRRTM4 or its presynaptic partner HSPG may contribute to cognitive disorders in rare cases. Our results identifying cell-type-specific functions and distinct presynaptic molecular pathways for different LRRTM family members reveal an unexpected complexity in the design of synapse-organizing protein networks and emphasize the importance of studying region-specific roles of individual gene products in brain function and dysfunction.

EXPERIMENTAL PROCEDURES

Further details are provided in the Supplemental Experimental Procedures.

Cell Culture, Recombinant Protein Production, and Cell Binding Assays

Dissociated rat or mouse primary hippocampal neuron cultures were prepared from embryonic day 18 rat embryos essentially as described before in Kaech and Banker (2006) and She and Craig (2011). Rat neurons were plated at a final density of 300,000 cells, while mouse neurons were plated at a final density of 500,000 cells per dish. For neuron coculture assays, either untransfected neurons or neurons transfected with 4–5 μg DNA at DIV0 using nucleofection (AMAXA Biosystems) and seeded at a density of one million per 60 mm dish were used for coculture assays as described in Graf et al. (2004). For heparinase treatment of COS7-neuron cocultures, coverslips were incubated with or without the glial feeder layers in conditioned media for 20–24 hr with or without 0.2 to 0.4 U/ml each of Heparinase I, II, and III cocktail. Soluble Fc or AP fusion proteins were prepared from stable or transiently expressing HEK293T cells. Cell binding assays were performed in EGB buffer (containing 168 mM NaCl, 2.6 mM KCl, 10 mM HEPES [pH 7.2], 2 mM $CaCl_2$, 2 mM $MgCl_2$, 10 mM D-glucose, and 100 μg/ml BSA) at 4°C essentially as described in Siddiqui et al. (2010). Binding assays with Myc-GPC5-AP or Myc-GPC5ΔGAG-AP were carried out with or without heparinase treatment.

Brain Affinity Chromatography

Brain affinity chromatography was performed with a crude synaptosomal fraction and followed a protocol similar to one described previously in Sugita et al. (2001). Protein G-Sepharose containing LRRTM4-Fc or Fc control was incubated with the synaptosomal extract overnight at 4°C, washed in extraction buffer, and sequentially eluted in extraction buffer containing 0.2 M NaCl, 0.5 M NaCl, 1.0 M NaCl, 1.0 M NaCl + 5 mM EGTA, and 0.2 M glycine (pH 2.4), neutralized by Tris-HCl (pH 8.6) after elution. Eluted proteins were precipitated with 20% TCA overnight at 4°C, washed with cold acetone, resuspended in sample buffer, and analyzed by SDS-PAGE gel followed by Sypro-ruby stain. Appropriate bands present in the LRRTM4-Fc eluate but not in the Fc eluate from the 0.5 M NaCl elution were excised and analyzed by LC-MS mass spectrometry.

Generation of *LRRTM4*$^{-/-}$ Mice

All animal experiments were compliant with government and institutional guidelines. The targeting vector was generated by the recombineering method (Liu et al., 2003) from a 129S7 bMQ BAC clone, specifically bMQ30G17 from the Sanger Institute (Adams et al., 2005), and was confirmed by sequencing. The targeting vector contains a LoxP site and a neomycin cassette flanked by Frt sites, replacing the major coding exon, Exon2, and a herpes simplex virus thymidine kinase expression cassette for negative selection. Targeting vector linearized by NotI was electroporated into 129/Ola embryonic stem (ES) cells for homologous recombination (Augustin et al., 1999; Thomas and Capecchi, 1987). Positive selection of ES cells was in the presence of G418 and negative selection against random integration by Gancyclovir. Homologous recombination was verified by Southern blot analysis with a probe 5′ to the targeting vector. Positive ES cells were further expanded and a single Neo cassette insertion was verified by Southern blotting against a probe for the Neo cassette after two independent restriction digestions, by EcoRV and BglII. Positive clones were injected into C57BL/6J blastocysts, which were implanted into surrogate female mice. Founder chimeras were backcrossed six to seven generations with C57BL/6J mice. Genotypes were regularly ascertained by PCR analysis.

Immunocytochemistry and Tissue Immunofluorescence

Neurons, COS7 cells, and cocultures were fixed for 12–15 min with warm 4% formaldehyde and 4% sucrose in PBS (pH 7.4) followed by permeabilization with 0.25% Triton X-100, except where live staining or staining of unpermeabilized fixed cultures was used. Live stainings were followed by fixation with warm 4% formaldehyde/4% sucrose in PBS (pH 7.4). Fixed cultures were then blocked in 10% BSA in PBS for 30 min at 37°C and primary antibodies applied in 3% BSA in PBS. After overnight incubation at 4°C, the coverslips were washed with PBS and incubated in secondary antibodies in 3% BSA in PBS for 1 hr at 37°C. The coverslips were then washed and mounted in elvanol (Tris-HCl, glycerol, and polyvinyl alcohol, with 2% 1,4-diazabicyclo[2,2,2] octane).

Immunofluorescence studies on coronal cryostat sections 20 μm thick at hippocampal level were performed on 6-week-old perfused *LRRTM4*$^{-/-}$ and littermate wild-type male mice. Fresh frozen sections were fixed by incubating in cold methanol for 10 min or for 7 min in 4% formaldehyde/4% sucrose and then blocked for 1 hr, followed by successive incubations with primary and secondary antibodies.

Immunoblotting

For all samples, protein concentrations were normalized and run on 10% polyacrylamide gels. Gels were transferred onto Immobilon P membranes (Millipore), which were blocked in 5% skim milk in Tris-buffered saline/0.05% Tween-20 or 5% BSA in PBS and incubated primary antibodies followed by secondary antibodies. Immunoblots were detected using the SuperSignal Chemiluminescent kit (Thermo Scientific) and a Bio-Rad gel documentation system or the Odyssey Li-COR fluorescence infrared system (Li-COR Bioscience).

Immunoprecipitation

Mouse brain crude synatosomal fraction was solubilized in Complexiolyte-48 (Logopharm). The protein amount was adjusted to 1–1.5 mg/ml, and the insoluble material was removed by centrifugation for 30 min at 22,000 × *g*. Purified antibody or antisera corresponding to 5 μg IgG per ml solution was added, and incubation was carried out for 4–6 hr at 4°C. Protein G-Sepharose suspension, 50 μl (GE Healthcare), was added and incubated overnight. The beads were collected by centrifugation and washed four times in Complexiolyte-48 dilution buffer before elution with sample buffer containing SDS and β-mercaptoethanol.

Golgi Staining

Golgi stainings for determining the spine density of different hippocampal regions were done using the FD Rapid GolgiStain Kit (FD NeuroTechnologies), essentially as recommended by the manufacturers. Spines were counted manually on a specific dendrite all the while altering the focal plane, and an image of the dendrite analyzed was acquired to determine its length.

Electrophysiological Studies

Whole-cell and extracellular recordings were performed with a MultiClamp 700B amplifier using WinLTP software. Using a Cs-methanesulfonate-based intracellular solution, mEPSCs were recorded under voltage clamp at −60 mV in the presence of tetrodotoxin (TTX) and bicuculline. Frequency

and amplitude were analyzed using MiniAnalysis software. GraphPad InStat and SigmaPlot were used for statistical analyses. Extracellular recordings to measure paired-pulsed facilitation and input-output responses were conducted in dentate gyrus molecualr layer while stimulating perforant path fibers. The initial slope of the fEPSP was measured to quantify synaptic strength (Johnston and Wu, 1995).

SUPPLEMENTAL INFORMATION

Supplemental Information includes Supplemental Experimental Procedures, six figures, and one table and can be found with this article online at http://dx.doi.org/10.1016/j.neuron.2013.06.029.

ACKNOWLEDGMENTS

We thank Xiling Zhou and Nazarine Fernandes for excellent technical assistance, Sarah Au-Yeung for contributions to the western blot analysis, Michiko Takeda for contributions to mouse colony management, Andrea Betz for advice on ES cell culture and Southern blotting, and Suzanne Perry and the team at the Proteomics Core Facility at the University of British Columbia. This work was supported by Canadian Institutes of Health Research Grants MOP-84241 and MOP-125967 and a Canada Research Chair salary award (A.M.C.), by a Michael Smith Foundation for Health Research Fellowship and an EMBO Short-Term Fellowship (T.J.S.), by the German Research Foundation (SPP1365/KA3423/1-1; H.K and N.B.), by the European Commission EUROSPIN and SynSys Consortia (FP7-HEALTH-F2-2009-241498; FP7-HEALTH-F2-2009-242167; N.B.), by the European Commission Innovative Medicines Initiative (EU-AIMS FP7-115300; N.B.), and by the Fritz Thyssen Foundation (H.K.).

Accepted: June 18, 2013
Published: August 1, 2013

REFERENCES

Adams, D.J., Quail, M.A., Cox, T., van der Weyden, L., Gorick, B.D., Su, Q., Chan, W.I., Davies, R., Bonfield, J.K., Law, F., et al. (2005). A genome-wide, end-sequenced 129Sv BAC library resource for targeting vector construction. Genomics *86*, 753–758.

Allen, N.J., Bennett, M.L., Foo, L.C., Wang, G.X., Chakraborty, C., Smith, S.J., and Barres, B.A. (2012). Astrocyte glypicans 4 and 6 promote formation of excitatory synapses via GluA1 AMPA receptors. Nature *486*, 410–414.

Altar, C.A., Siuciak, J.A., Wright, P., Ip, N.Y., Lindsay, R.M., and Wiegand, S.J. (1994). In situ hybridization of trkB and trkC receptor mRNA in rat forebrain and association with high-affinity binding of [125I]BDNF, [125I]NT-4/5 and [125I] NT-3. Eur. J. Neurosci. *6*, 1389–1405.

Anggono, V., and Huganir, R.L. (2012). Regulation of AMPA receptor trafficking and synaptic plasticity. Curr. Opin. Neurobiol. *22*, 461–469.

Augustin, I., Rosenmund, C., Südhof, T.C., and Brose, N. (1999). Munc13-1 is essential for fusion competence of glutamatergic synaptic vesicles. Nature *400*, 457–461.

Betancur, C., Sakurai, T., and Buxbaum, J.D. (2009). The emerging role of synaptic cell-adhesion pathways in the pathogenesis of autism spectrum disorders. Trends Neurosci. *32*, 402–412.

Carrié, A., Jun, L., Bienvenu, T., Vinet, M.C., McDonell, N., Couvert, P., Zemni, R., Cardona, A., Van Buggenhout, G., Frints, S., et al. (1999). A new member of the IL-1 receptor family highly expressed in hippocampus and involved in X-linked mental retardation. Nat. Genet. *23*, 25–31.

de Wit, J., Sylwestrak, E., O'Sullivan, M.L., Otto, S., Tiglio, K., Savas, J.N., Yates, J.R., 3rd, Comoletti, D., Taylor, P., and Ghosh, A. (2009). LRRTM2 interacts with Neurexin1 and regulates excitatory synapse formation. Neuron *64*, 799–806.

DeNardo, L.A., de Wit, J., Otto-Hitt, S., and Ghosh, A. (2012). NGL-2 regulates input-specific synapse development in CA1 pyramidal neurons. Neuron *76*, 762–775.

Elias, G.M., Elias, L.A., Apostolides, P.F., Kriegstein, A.R., and Nicoll, R.A. (2008). Differential trafficking of AMPA and NMDA receptors by SAP102 and PSD-95 underlies synapse development. Proc. Natl. Acad. Sci. USA *105*, 20953–20958.

Ethell, I.M., Irie, F., Kalo, M.S., Couchman, J.R., Pasquale, E.B., and Yamaguchi, Y. (2001). EphB/syndecan-2 signaling in dendritic spine morphogenesis. Neuron *31*, 1001–1013.

Francks, C., Maegawa, S., Laurén, J., Abrahams, B.S., Velayos-Baeza, A., Medland, S.E., Colella, S., Groszer, M., McAuley, E.Z., Caffrey, T.M., et al. (2007). LRRTM1 on chromosome 2p12 is a maternally suppressed gene that is associated paternally with handedness and schizophrenia. Mol. Psychiatry *12*, 1129–1139, 1057.

Fransson, L.A., Belting, M., Cheng, F., Jönsson, M., Mani, K., and Sandgren, S. (2004). Novel aspects of glypican glycobiology. Cell. Mol. Life Sci. *61*, 1016–1024.

Graf, E.R., Zhang, X., Jin, S.X., Linhoff, M.W., and Craig, A.M. (2004). Neurexins induce differentiation of GABA and glutamate postsynaptic specializations via neuroligins. Cell *119*, 1013–1026.

Gruenheid, S., Gatzke, L., Meadows, H., and Tufaro, F. (1993). Herpes simplex virus infection and propagation in a mouse L cell mutant lacking heparan sulfate proteoglycans. J. Virol. *67*, 93–100.

Harris, K.M., and Kater, S.B. (1994). Dendritic spines: cellular specializations imparting both stability and flexibility to synaptic function. Annu. Rev. Neurosci. *17*, 341–371.

Hsueh, Y.P., Yang, F.C., Kharazia, V., Naisbitt, S., Cohen, A.R., Weinberg, R.J., and Sheng, M. (1998). Direct interaction of CASK/LIN-2 and syndecan heparan sulfate proteoglycan and their overlapping distribution in neuronal synapses. J. Cell Biol. *142*, 139–151.

Irie, F., Badie-Mahdavi, H., and Yamaguchi, Y. (2012). Autism-like socio-communicative deficits and stereotypies in mice lacking heparan sulfate. Proc. Natl. Acad. Sci. USA *109*, 5052–5056.

Johnson, K.G., Tenney, A.P., Ghose, A., Duckworth, A.M., Higashi, M.E., Parfitt, K., Marcu, O., Heslip, T.R., Marsh, J.L., Schwarz, T.L., et al. (2006). The HSPGs Syndecan and Dallylike bind the receptor phosphatase LAR and exert distinct effects on synaptic development. Neuron *49*, 517–531.

Johnston, D., and Wu, S.-S. (1995). Foundations of Cellular Neurophysiology (Cambridge: MIT Press).

Kaech, S., and Banker, G. (2006). Culturing hippocampal neurons. Nat. Protoc. *1*, 2406–2415.

Kim, S., Burette, A., Chung, H.S., Kwon, S.K., Woo, J., Lee, H.W., Kim, K., Kim, H., Weinberg, R.J., and Kim, E. (2006). NGL family PSD-95-interacting adhesion molecules regulate excitatory synapse formation. Nat. Neurosci. *9*, 1294–1301.

Ko, J., Fuccillo, M.V., Malenka, R.C., and Südhof, T.C. (2009). LRRTM2 functions as a neurexin ligand in promoting excitatory synapse formation. Neuron *64*, 791–798.

Krueger, D.D., Tuffy, L.P., Papadopoulos, T., and Brose, N. (2012). The role of neurexins and neuroligins in the formation, maturation, and function of vertebrate synapses. Curr. Opin. Neurobiol. *22*, 412–422.

Laurén, J., Airaksinen, M.S., Saarma, M., and Timmusk, T. (2003). A novel gene family encoding leucine-rich repeat transmembrane proteins differentially expressed in the nervous system. Genomics *81*, 411–421.

Lauri, S.E., Kaukinen, S., Kinnunen, T., Ylinen, A., Imai, S., Kaila, K., Taira, T., and Rauvala, H. (1999). Reg1ulatory role and molecular interactions of a cell-surface heparan sulfate proteoglycan (N-syndecan) in hippocampal long-term potentiation. J. Neurosci. *19*, 1226–1235.

Lein, E.S., Hawrylycz, M.J., Ao, N., Ayres, M., Bensinger, A., Bernard, A., Boe, A.F., Boguski, M.S., Brockway, K.S., Byrnes, E.J., et al. (2007). Genome-wide atlas of gene expression in the adult mouse brain. Nature *445*, 168–176.

Li, H., Yamagata, T., Mori, M., and Momoi, M.Y. (2002). Association of autism in two patients with hereditary multiple exostoses caused by novel deletion mutations of EXT1. J. Hum. Genet. *47*, 262–265.

Linhoff, M.W., Laurén, J., Cassidy, R.M., Dobie, F.A., Takahashi, H., Nygaard, H.B., Airaksinen, M.S., Strittmatter, S.M., and Craig, A.M. (2009). An unbiased expression screen for synaptogenic proteins identifies the LRRTM protein family as synaptic organizers. Neuron *61*, 734–749.

Liu, P., Jenkins, N.A., and Copeland, N.G. (2003). A highly efficient recombineering-based method for generating conditional knockout mutations. Genome Res. *13*, 476–484.

Lu, W., Man, H., Ju, W., Trimble, W.S., MacDonald, J.F., and Wang, Y.T. (2001). Activation of synaptic NMDA receptors induces membrane insertion of new AMPA receptors and LTP in cultured hippocampal neurons. Neuron *29*, 243–254.

Lucido, A.L., Suarez Sanchez, F., Thostrup, P., Kwiatkowski, A.V., Leal-Ortiz, S., Gopalakrishnan, G., Liazoghli, D., Belkaid, W., Lennox, R.B., Grutter, P., et al. (2009). Rapid assembly of functional presynaptic boutons triggered by adhesive contacts. J. Neurosci. *29*, 12449–12466.

Malinow, R., and Malenka, R.C. (2002). AMPA receptor trafficking and synaptic plasticity. Annu. Rev. Neurosci. *25*, 103–126.

Michaelson, J.J., Shi, Y., Gujral, M., Zheng, H., Malhotra, D., Jin, X., Jian, M., Liu, G., Greer, D., Bhandari, A., et al. (2012). Whole-genome sequencing in autism identifies hot spots for de novo germline mutation. Cell *151*, 1431–1442.

Ohmi, K., Zhao, H.Z., and Neufeld, E.F. (2011). Defects in the medial entorhinal cortex and dentate gyrus in the mouse model of Sanfilippo syndrome type B. PLoS ONE *6*, e27461.

Pinto, D., Pagnamenta, A.T., Klei, L., Anney, R., Merico, D., Regan, R., Conroy, J., Magalhaes, T.R., Correia, C., Abrahams, B.S., et al. (2010). Functional impact of global rare copy number variation in autism spectrum disorders. Nature *466*, 368–372.

Scheiffele, P., Fan, J., Choih, J., Fetter, R., and Serafini, T. (2000). Neuroligin expressed in nonneuronal cells triggers presynaptic development in contacting axons. Cell *101*, 657–669.

Schwenk, J., Harmel, N., Brechet, A., Zolles, G., Berkefeld, H., Müller, C.S., Bildl, W., Baehrens, D., Hüber, B., Kulik, A., et al. (2012). High-resolution proteomics unravel architecture and molecular diversity of native AMPA receptor complexes. Neuron *74*, 621–633.

She, K., and Craig, A.M. (2011). NMDA receptors mediate synaptic competition in culture. PLoS ONE *6*, e24423.

Shen, K., and Scheiffele, P. (2010). Genetics and cell biology of building specific synaptic connectivity. Annu. Rev. Neurosci. *33*, 473–507.

Siddiqui, T.J., and Craig, A.M. (2011). Synaptic organizing complexes. Curr. Opin. Neurobiol. *21*, 132–143.

Siddiqui, T.J., Pancaroglu, R., Kang, Y., Rooyakkers, A., and Craig, A.M. (2010). LRRTMs and neuroligins bind neurexins with a differential code to cooperate in glutamate synapse development. J. Neurosci. *30*, 7495–7506.

Soler-Llavina, G.J., Fuccillo, M.V., Ko, J., Südhof, T.C., and Malenka, R.C. (2011). The neurexin ligands, neuroligins and leucine-rich repeat transmembrane proteins, perform convergent and divergent synaptic functions in vivo. Proc. Natl. Acad. Sci. USA *108*, 16502–16509.

Südhof, T.C. (2008). Neuroligins and neurexins link synaptic function to cognitive disease. Nature *455*, 903–911.

Sugita, S., Saito, F., Tang, J., Satz, J., Campbell, K., and Südhof, T.C. (2001). A stoichiometric complex of neurexins and dystroglycan in brain. J. Cell Biol. *154*, 435–445.

Takahashi, H., Arstikaitis, P., Prasad, T., Bartlett, T.E., Wang, Y.T., Murphy, T.H., and Craig, A.M. (2011). Postsynaptic TrkC and presynaptic PTPσ function as a bidirectional excitatory synaptic organizing complex. Neuron *69*, 287–303.

Takahashi, H., Katayama, K., Sohya, K., Miyamoto, H., Prasad, T., Matsumoto, Y., Ota, M., Yasuda, H., Tsumoto, T., Aruga, J., and Craig, A.M. (2012). Selective control of inhibitory synapse development by Slitrk3-PTPδ trans-synaptic interaction. Nat. Neurosci. *15*, 389–398, S1–S2.

Thomas, K.R., and Capecchi, M.R. (1987). Site-directed mutagenesis by gene targeting in mouse embryo-derived stem cells. Cell *51*, 503–512.

Trommald, M., and Hulleberg, G. (1997). Dimensions and density of dendritic spines from rat dentate granule cells based on reconstructions from serial electron micrographs. J. Comp. Neurol. *377*, 15–28.

Van Vactor, D., Wall, D.P., and Johnson, K.G. (2006). Heparan sulfate proteoglycans and the emergence of neuronal connectivity. Curr. Opin. Neurobiol. *16*, 40–51.

Varoqueaux, F., Aramuni, G., Rawson, R.L., Mohrmann, R., Missler, M., Gottmann, K., Zhang, W., Südhof, T.C., and Brose, N. (2006). Neuroligins determine synapse maturation and function. Neuron *51*, 741–754.

Westerink, R.H., Beekwilder, J.P., and Wadman, W.J. (2012). Differential alterations of synaptic plasticity in dentate gyrus and CA1 hippocampal area of Calbindin-D28K knockout mice. Brain Res. *1450*, 1–10.

Willour, V.L., Seifuddin, F., Mahon, P.B., Jancic, D., Pirooznia, M., Steele, J., Schweizer, B., Goes, F.S., Mondimore, F.M., Mackinnon, D.F., et al.; Bipolar Genome Study Consortium. (2012). A genome-wide association study of attempted suicide. Mol. Psychiatry *17*, 433–444.

Woo, J., Kwon, S.K., Choi, S., Kim, S., Lee, J.R., Dunah, A.W., Sheng, M., and Kim, E. (2009). Trans-synaptic adhesion between NGL-3 and LAR regulates the formation of excitatory synapses. Nat. Neurosci. *12*, 428–437.

Wu, H., Xiong, W.C., and Mei, L. (2010). To build a synapse: signaling pathways in neuromuscular junction assembly. Development *137*, 1017–1033.

Xu, W. (2011). PSD-95-like membrane associated guanylate kinases (PSD-MAGUKs) and synaptic plasticity. Curr. Opin. Neurobiol. *21*, 306–312.

Yamaguchi, Y. (2001). Heparan sulfate proteoglycans in the nervous system: their diverse roles in neurogenesis, axon guidance, and synaptogenesis. Semin. Cell Dev. Biol. *12*, 99–106.

Yoshida, T., Yasumura, M., Uemura, T., Lee, S.J., Ra, M., Taguchi, R., Iwakura, Y., and Mishina, M. (2011). IL-1 receptor accessory protein-like 1 associated with mental retardation and autism mediates synapse formation by trans-synaptic interaction with protein tyrosine phosphatase δ. J. Neurosci. *31*, 13485–13499.

Yoshida, T., Shiroshima, T., Lee, S.J., Yasumura, M., Uemura, T., Chen, X., Iwakura, Y., and Mishina, M. (2012). Interleukin-1 receptor accessory protein organizes neuronal synaptogenesis as a cell adhesion molecule. J. Neurosci. *32*, 2588–2600.

Yuzaki, M. (2011). Cbln1 and its family proteins in synapse formation and maintenance. Curr. Opin. Neurobiol. *21*, 215–220.